Frontiers of Information Technology & Electronic Engineering
www.jzus.zju.edu.cn; engineering.cae.cn; www.springerlink.com
ISSN 2095-9184 (print); ISSN 2095-9230 (online)
E-mail: jzus@zju.edu.cn

Review:

Near-field communications: characteristics, technologies, and engineering*

Yajun ZHAO[†1,2], Linglong DAI[†‡3], Jianhua ZHANG[†‡4], Ran JI[5], Mengnan JIAN[1,2], Hao XUE[6,7], Hongkang YU[1,2], Yunqi SUN[1,2], Yu LU[3], Zidong WU[3], Zhuo XU[3], Jinke LI[3], Haiyang MIAO[4], Zhiqiang YUAN[4], Pan TANG[4], Jiayu SHEN[5], Tierui GONG[5], Haixia LIU[6,7], Jiaqi HAN[6,7], Qiang FENG[6,7], Zhi CHEN[8], Lingxiang LI[8], Gang YANG[8], Yong ZENG[9,10], Cunhua PAN[9], Wang LIU[9], Kangda ZHI[11], Weidong HU[12], Yuanwei LIU[13], Xidong MU[14], Chau YUEN[15], Mérouane DEBBAH[16], Chongwen HUANG[†‡5], Long LI[†‡6,7], Ping ZHANG[†‡4]

[1]*State Key Laboratory of Mobile Network and Mobile Multimedia Technology, Shenzhen 518055, China*

[2]*ZTE Corporation, Beijing 100192, China*

[3]*Department of Electronic Engineering, Tsinghua University, Beijing 100084, China*

[4]*State Key Laboratory of Networking and Switching Technology, Beijing University of Posts and Telecommunications, Beijing 100876, China*

[5]*College of Information Science and Electronic Engineering, Zhejiang University, Hangzhou 310007, China*

[6]*Key Laboratory of High Speed Circuit Design and EMC of Ministry of Education, School of Electronic Engineering, Xidian University, Xi'an 710071, China*

[7]*Collaborative Innovation Center of Information Sensing and Understanding, Xidian University, Xi'an 710071, China*

[8]*National Key Laboratory of Wireless Communications, University of Electronic Science and Technology of China, Chengdu 611731, China*

[9]*National Mobile Communications Research Laboratory, Southeast University, Nanjing 210096, China*

[10]*Purple Mountain Laboratories, Nanjing 211111, China*

[11]*School of Electrical Engineering and Computer Science, Technical University of Berlin, Berlin 10623, Germany*

[12]*School of Integrated Circuits and Electronics, Beijing Institute of Technology, Beijing 100081, China*

[13]*Department of Electrical and Electronic Engineering, The University of Hong Kong, Hong Kong, China*

[14]*Centre for Wireless Innovation (CWI), School of Electronics, Electrical Engineering and Computer Science, Queen's University Belfast, Belfast BT3 9DT, UK*

[15]*School of Electrical and Electronic Engineering, Nanyang Technological University, Singapore 639798, Singapore*

[16]*KU 6G Research Center, Khalifa University of Science and Technology, Abu Dhabi, United Arab Emirates*

[†]E-mail: zhao.yajun1@zte.com.cn; daill@tsinghua.edu.cn; jhzhang@bupt.edu.cn; chongwenhuang@zju.edu.cn; lilong@mail.xidian.edu.cn; pzhang@bupt.edu.cn

Received July 8, 2024; Revision accepted Oct. 25, 2024; Crosschecked Nov. 18, 2024

[‡] Corresponding authors

* Project supported by the Natural Science Foundation of Hunan Province, China (No. 2022JJ40561), the Scientific Research Program of National University of Defense Technology, China (No. ZK22-46), and the National Natural Science Foundation of China (Nos. 61890542, 62001481, and 62071475)

ORCID: Yajun ZHAO, https://orcid.org/0000-0001-8823-5282; Linglong DAI, https://orcid.org/0000-0002-4250-7315; Jianhua ZHANG, https://orcid.org/0000-0002-6492-3846; Chongwen HUANG, https://orcid.org/0000-0001-8398-8437; Long LI, https://orcid.org/0000-0003-0472-7314; Ping ZHANG, https://orcid.org/0000-0002-1485-5849

Abstract: Near-field technology is increasingly recognized due to its transformative potential in communication systems, establishing it as a critical enabler for sixth-generation (6G) telecommunication development. This paper presents a comprehensive survey of recent advancements in near-field technology research. First, we explore the near-field propagation fundamentals by detailing definitions, transmission characteristics, and performance analysis. Next, we investigate various near-field channel models—deterministic, stochastic, and electromagnetic information theory based models, and review the latest progress in near-field channel testing, highlighting practical performance and limitations. With evolving channel models, traditional mechanisms such as channel estimation, beamtraining, and codebook design require redesign and optimization to align with near-field propagation characteristics. We then introduce innovative beam designs enabled by near-field technologies, focusing on non-diffractive beams (such as Bessel and Airy) and orbital angular momentum (OAM) beams, addressing both hardware architectures and signal processing frameworks, showcasing their revolutionary potential in near-field communication systems. Additionally, we highlight progress in both engineering and standardization, covering the primary 6G spectrum allocation, enabling technologies for near-field propagation, and network deployment strategies. Finally, we conclude by identifying promising future research directions for near-field technology development that could significantly impact system design. This comprehensive review provides a detailed understanding of the current state and potential of near-field technologies.

Key words: 6G; Near-field technology; Channel model; Codebook; Non-diffractive beams; Orbital angular momentum; Engineering and standardization

https://doi.org/10.1631/FITEE.2400576 **CLC number:** TN929.5

1 Introduction

The global deployment of fifth-generation (5G) mobile has catalyzed research into sixth-generation (6G) communication technologies to address emerging demands in immersive communication as well as in intelligent and ubiquitous connectivity (Zhao et al., 2019; Yuan YF et al., 2020; IMT-2030 (6G) Promotion Group, 2022). The International Telecommunication Union (ITU)'s release of the 6G vision, future technology trends, and framework in June 2023 initiated formal standardization (ITU-R WP 5D, 2023), defining six major application scenarios: immersive communication, hyper reliable and low-latency communication, massive communication, ubiquitous connectivity, artificial intelligence (AI) and communication, and integrated sensing and communication (ISAC). Sixth-generation networks target a tenfold improvement over 5G networks in peak data rates, latency reduction, reliability, and connection density (Zhou Z et al., 2015; Cui TJ et al., 2021).

Key 6G candidate technologies include extremely large-scale antenna array (ELAA) (Cui MY and Dai, 2024; Liu ZL et al., 2024; Lu HQ et al., 2024), ISAC (Ouyang et al., 2022), reconfigurable intelligent surface (RIS) (Cheng et al., 2023; Zhao, 2023), and new mid-band (Zhang JH et al., 2024b) and terahertz (THz) communication technologies (Mukherjee and Gupta, 2008). ELAA, evolving from massive multiple-input multiple-output (MIMO), increases the number of antennas to enhance spectral efficiency and spatial resolution for wireless communication and sensing. This technology encompasses ultra-massive MIMO (UM-MIMO), cell-free massive MIMO, and RIS, making it critical for meeting 6G networks' technical benchmarks, such as peak data rates, spectral efficiency, positioning and sensing accuracy, and high connection density.

Sixth-generation networks will use higher-frequency bands (above 6 GHz), including U6G (6.425–7.125 GHz), mid-band (7–24 GHz), millimeter-wave (mmWave), and sub-THz bands. These frequency ranges offer expanded bandwidths and improved propagation characteristics, effectively enabling next-generation cellular networks.

However, the transition from massive MIMO to ELAA, coupled higher-frequency bands, involves more than just an increase in the number of antennas or array dimensions; it fundamentally alters electromagnetic (EM) propagation characteristics. The integration leads to a shift from traditional uniform plane-wave (UPW) propagation in the far field to non-uniform spherical wave (NUSW) propagation in the near field, as well as a transition from spatial stationarity to spatial non-stationarity (SnS) (Nepa and Buffi, 2017; Björnson et al., 2021; Cui MY and Dai, 2022; Hu S et al., 2022; Cui MY et al., 2023a).

In particular, multipath wavefronts impinging on the array can no longer be approximated as planar due to near-field propagation properties. SnS phenomena

may emerge in near-field MIMO systems, where different spatial channels can be observed by array elements at varying spatial locations. Limited-sized objects within the propagation environment may no longer serve as complete scatterers for the entire array with a large aperture. These unique properties significantly impact channel capacity and beamforming performance in near-field MIMO systems, underscoring the need to account for them in channel models to ensure accurate system evaluation. Some channel models that account for near-field properties and SnS have been reported in the literature (Dong and Zeng, 2022; Lu HQ et al., 2024). With channel model evolution, traditional mechanisms based on far-field assumptions—channel estimation, beam training, codebook design, and beamforming—need redesign and optimization to align with near-field propagation characteristics. Existing reviews (Liu YW et al., 2023a; Lu HQ et al., 2024) have systematically summarized research in near-field technologies, highlighting their importance and advancements across various applications. Additionally, a white paper (Zhao et al., 2024) comprehensively explored potential application scenarios for near-field technologies, identifying 14 distinct near-field application types with particular emphasis on near-field ISAC, wireless power transfer, and multiple accesses.

The emergence of near-field propagation has sparked significant interest in novel beam types, notably non-diffractive beams (Bessel (McGloin and Dholakia, 2005) and Airy) and orbital angular momentum (OAM) beams. Research on non-diffractive beams based on higher-order Bessel functions to enhance OAM communications has shown promise (Lian et al., 2022).

While near-field technologies have made substantial progress in academic research, engineering, and standardization, a comprehensive review addressing the engineering and standardization aspects is still lacking.

This review presents a detailed survey of the recent advancements in near-field communication research, with key contributions outlined as follows:

First, we examine near-field channel models and measurement results, covering deterministic, stochastic, and EM information theory based models. We provide insights into the latest progress in channel testing, detailing the practical performance and limitations of these models.

Second, we provide a thorough analysis of channel state information (CSI) acquisition mechanisms tailored to near-field communications, encompassing channel estimation, beam training, and codebook design.

Third, we introduce novel beams enabled by near-field effects, including non-diffractive beams (Bessel beams and Airy beams) and OAM beams, discussing their hardware architecture and signal processing workflow, highlighting their transformative potential in near-field communication systems.

Fourth, we highlight engineering and standardization progress, exploring key topics including the primary 6G spectrum and enabling technologies for near-field propagation and network deployment strategies.

Finally, we introduce several future research directions related to near-field technologies, with potential to significantly impact system design.

The structure of this survey is illustrated in Fig. 1. Section 2 delves into the characteristics of near-field propagation, focusing on definitions, transmission characteristics, and performance analysis. Section 3 examines near-field channel models and measurement results, covering deterministic, stochastic, and EM information theory based models. We also review recent advancements in near-field channel test, providing insights into the practical performance and limitations of these models. Section 4 addresses the evolution of channel models, emphasizing the need to redesign and optimize mechanisms such as channel estimation, beam training, codebook design, and beamforming, to align with the distinct characteristics of near-field propagation. Section 5 introduces innovative beam designs facilitated by near-field technologies, including Bessel, Airy, and OAM beams. We examine their hardware architectures and signal processing workflows, emphasizing their potential to transform near-field communication systems. Section 6 focuses on the significant progress made in engineering and standardization, with an emphasis on key areas such as the primary 6G spectrum, enabling technologies for near-field propagation, network deployment, and standardization efforts. Several promising directions for future research in near-field technologies are discussed in Section 7. Finally, Section 8 concludes the paper.

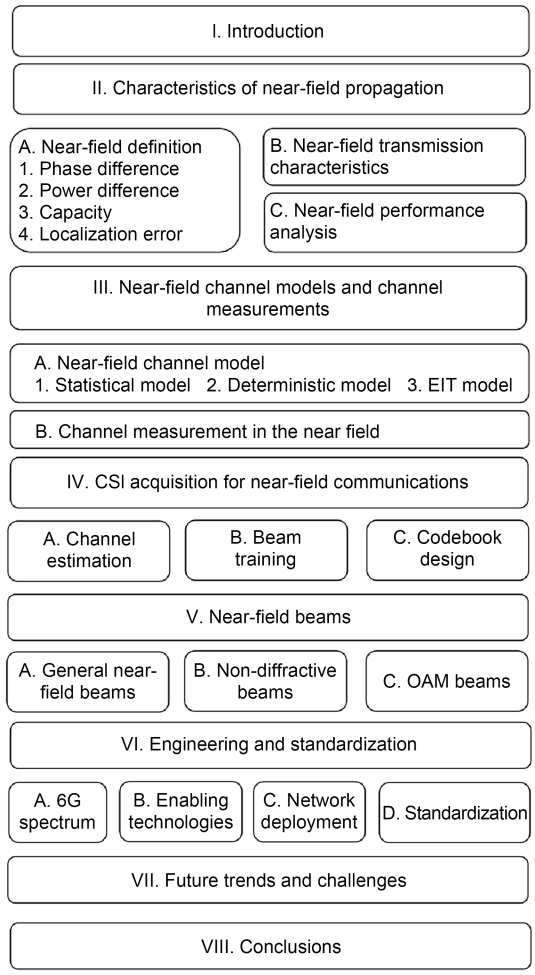

Fig. 1 Structure of the survey

2 Characteristics of near-field propagation

2.1 Near-field definition

This subsection introduces the key distinctions between far-field and near-field communications, followed by near-field communication definition and its applicable scenarios.

As depicted in Fig. 2, according to the EM and antenna theory, the fields surrounding a transmitter comprise near-field and far-field regions, with the near-field region being further categorized into the reactive and radiative regions (Yaghjian, 1986). The reactive near-field region exists close to the antenna, within the Fresnel distance, while the radiative near-field region extends a few wavelengths from the antenna, between the Fresnel and Rayleigh distances.

EM wave amplitudes vary smoothly across different antennas in an array in the radiative near-field

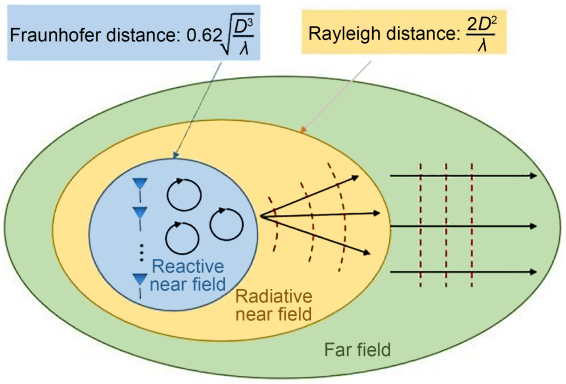

Fig. 2 Boundaries of various propagation regions and characteristics of near-field and far-field wavefronts

region, while phase shifts increase significantly and exponentially with the increasing antenna index (Ramezani et al., 2023). As a result, the signal propagation model in this region must be described using a spherical wave model. In contrast, the far-field region allows a simpler plane wave approximation. The aforementioned introduction presents the commonly accepted definitions of near-field regions in the literature. Beyond the prevalent phase-based definition, the near-field range can also be defined through perspectives of phase and power differences, channel capacity, and localization error. The following subsections outline near-field communication definitions from these four perspectives.

2.1.1 Phase difference perspective

The classic boundary between the near-field and far-field regions is defined by the Fraunhofer or Rayleigh distance (Selvan and Janaswamy, 2017), where the maximum phase difference between the spherical and plane wave models does not exceed π/8. This distance is given by $2D^2/\lambda$, where D represents the maximum aperture of the antenna and λ denotes the carrier wavelength. If the user is beyond the Rayleigh distance from the base station (BS), signal propagation can be approximated as plane waves (far-field region). Within the Rayleigh distance, the user is in the near-field region.

2.1.2 Power difference perspective

While the maximum ratio combining (MRC) technique can theoretically align phases to neutralize their impact on the received power, phase differences may not be completely eliminated on practical

implementation due to imperfect channel estimation and may result in power losses. To address this, Cui MY and Dai (2024) introduced the concept of effective Rayleigh distance to better characterize the near-field boundary.

Once phase impacts on the received power are mitigated via MRC, the received power is predominantly influenced by amplitude response differences among antenna elements. Critical distance and uniform-power distance were proposed (Lu HQ and Zeng, 2021, 2022) to define the near-field range based on power differences, considering the amplitude variations within the same transmitter antenna array. Specifically, the boundary was defined, where the power ratio between the weakest and strongest antenna elements detected at the receiver exceeds a certain threshold. The impact of power differences in the near-field region was further analyzed (Zhi et al., 2024) using an EM channel model.

The critical distance is determined by the antenna aperture, characterizing the near-field boundary along the antenna aperture axis. Uniform-power distance incorporates additional factors such as structure and projected aperture of the antenna array, providing a more precise off-axis near-field boundary description. Li RW et al. (2023) further derived equal-power lines and surfaces for the near-field region using uniform linear array (ULA) and uniform circular planar array (UCPA) structures.

2.1.3 Capacity perspective

Channel capacity metrics offer another perspective on near-field boundaries, incorporating channel capacity (Jiang JS and Ingram, 2005), eigenvalues (Bohagen et al., 2009), rank (Li RW et al., 2023), multi-stream transmission characteristics (Wang P et al., 2014), and effective degrees of freedom (EDoFs) (Sun et al., 2023), to evaluate the applicable areas of far-field plane waves and near-field spherical waves. Li RW et al. (2023) suggested determining the boundary of the near-field region using the equip-rank surface. This study demonstrates that the near-field range expands with the increasing number of scatterers in both line-of-sight (LoS) and non-line-of-sight (NLoS) environments, with stronger effects in NLoS conditions.

To assess spatial reuse, Wang P et al. (2014) introduced the effective reuse distance metric, $D_{\max}^{(m)}$, which represents the maximum distance at which the channel can effectively support m independent spatial streams at a given signal-to-noise ratio (SNR). Moreover, the near-field boundary from the perspective of multi-stream transmission was further explored by considering channel's EDoFs (Sun et al., 2023). This approach highlights the influence of antenna aperture and element number on the near-field range.

2.1.4 Localization error perspective

While the Fraunhofer distance is a rough estimate to distinguish the far-field and near-field regions, it may not suit localization applications as it overlooks critical factors such as angle of arrival (AoA), beam squint, and transmit power. Chen H et al. (2022) demonstrated that the Fraunhofer distance is inadequate for determining when to apply a more accurate near-field model instead of the far-field model due to potential model mismatch within its applicable range.

To address this, a new metric based on the mismatched Cramér–Rao bound (CRB) was proposed, suggesting that the boundary between the far-field and near-field regions be defined by the −3 dB contour of the model mismatch positioning error between the two regions.

2.2 Near-field transmission characteristics

Near-field communication exhibits several distinctive physical characteristics that fundamentally impact communication systems. These include tri-polarization (Wei et al., 2023), evanescent waves (Ji et al., 2023), beam splitting (Cui MY and Dai, 2024), beam focusing (Ramezani et al., 2023; Wu ZD and Dai, 2023; Wu ZD et al., 2023), SnS (Dong and Zeng, 2022), and various other distinctive physical properties. This subsection examines these unique characteristics and their applications in communication systems.

The tri-polarization effect emerges naturally in near-field communication from the rapid decay of the radial component in Maxwell's equations for dipole antennas. Wei et al. (2023) explored this effect by considering both the near-field spherical wave channel and the multi-polarization effect using a vector Green function (Fig. 3). This study further develops a polarization- and channel-oriented dual precoding technique for the multi-polarized near-field spherical wave channel. A systematic diagram illustrating these concepts was provided in their work. Simulation results revealed that this multi-polarization effect in

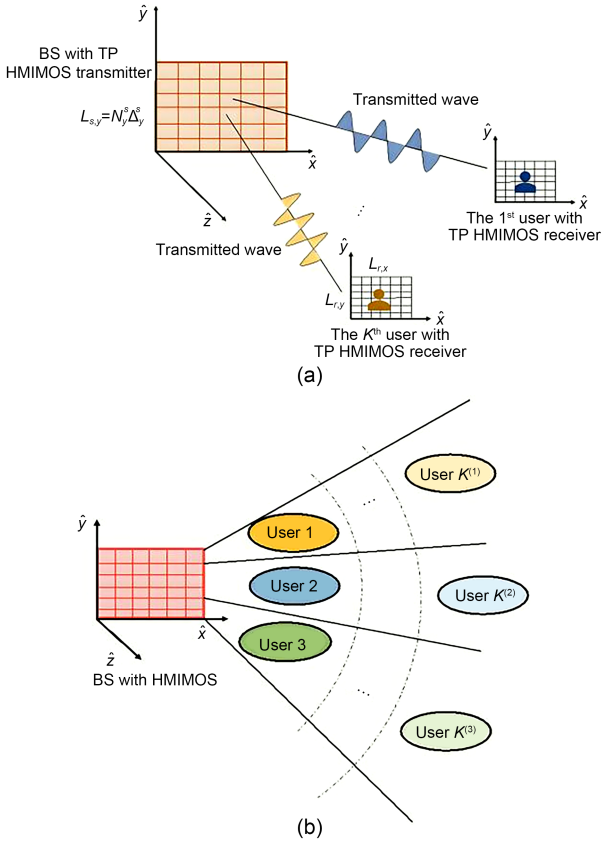

Fig. 3 Near-field multi-polarized spherical wave model (Wei et al., 2023): (a) the TP MU-HMIMOS downlink communication system; (b) the user cluster scheme in TP MU-HMIMOS systems

near-field communication can notably enhance system capacity within certain near-field ranges.

Near-field beam-splitting effect occurs notably in RIS applications. While phase shifter based beamformers effectively generate focused beams toward specific locations in narrowband systems, resulting in a beam focusing gain, they encounter challenges in broadband scenarios.

The nearly frequency-independent nature of the phase shifters causes spherical beams of different frequencies to concentrate on distinct physical locations, leading to near-field beam-splitting effect. This effect causes significant array gain loss as beams of varying frequencies fail to align with the target user at a specific position.

However, this effect also offers advantages by generating multiple spatial beams within the same frequency band. Users can control the angular coverage of beam transmission at different frequencies through system parameter design, facilitating rapid CSI acquisition

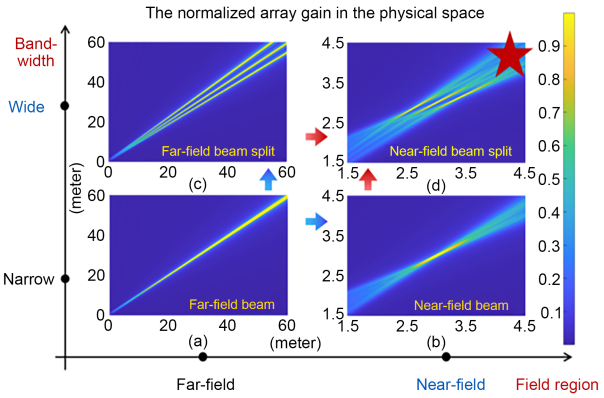

Fig. 4 Near-field beam-splitting effect schematic (Cui MY and Dai, 2024): (a) far-field narrowband scenario; (b) near-field narrowband scenario; (c) far-field wideband scenario; (d) near-field wideband scenario

in the far field and enabling swift beam training or tracking processes. Fig. 4 illustrates the spatial distribution of energy-focusing points in near-field broadband communication.

In the context of near-field beam focusing, there is a clear distinction in the abilities of plane and spherical waves to capture radiant energy from space. Plane waves serve as far-field approximation of spherical waves. In the far-field region, the phase of an EM wave can be approximated using a planar Taylor expansion, resulting in a clean linear phase that forms a plane wavefront, determined solely by the angle of incidence. This linear phase enables far-field beamforming, directing beam energy toward specific angles across varying distances, a process known as beam steering.

However, this linear phase characteristic of plane waves does not fully capture the complexity of spherical waves. In the near-field region, the phase of a spherical wave requires accurate derivation based on the physical antenna geometry, resulting in a nonlinear phase that depends on the antenna index. This nonlinear phase contains crucial information about both the angle of incidence and the distance for each path between the BS and the user equipment (UE). By using this detailed distance information within the spherical wavefront, near-field beamforming can focus beam energy precisely at designated locations, achieving energy concentration in both angle and distance dimensions. This capability has led to the term “beam focusing” as a synonymous concept for near-field beamforming. The characteristics of near-field beams

can be summarized in two key aspects: near-field distance-domain focusing for various arrays and distance-domain asymptotic orthogonality.

First, for the near-field distance-domain focusing, the depth-of-focus (DF) (Ramezani et al., 2023) at a transmitter distance F with matched filtering is given by

$$z \in \left[\frac{d_{\mathrm{FA}}F}{d_{\mathrm{FA}}+10F}, \frac{d_{\mathrm{FA}}F}{d_{\mathrm{FA}}-10F}\right], \tag{1}$$

where d_{FA} is the N-fold Rayleigh distance. The depth of the beam depends on the location where the matched filter is focused (Fig. 5). When the focus is within $d_{\mathrm{FA}}/10$, the near-field beam depth becomes finite.

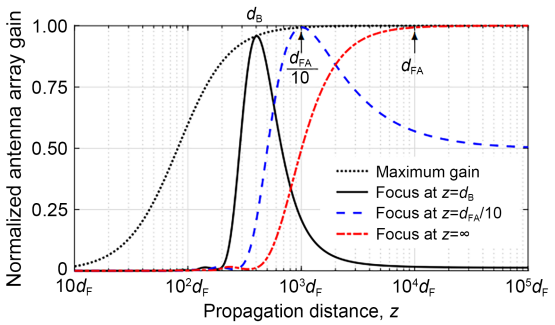

Fig. 5 Variations in beam gain with distance (Ramezani et al., 2023)

Near-field beam focusing can concentrate beam energy toward a precise location determined by both the angle and distance. To improve spectral efficiency using spatial distance-domain resources, Cui MY and Dai (2022) demonstrated the asymptotic orthogonality of near-field array response vectors, with the channel correlation expressed as follows:

$$f^{\mathrm{near}} \approx \left|\frac{C(\beta)+\mathrm{j}S(\beta)}{\beta}\right|, \tag{2}$$

where $\beta = \sqrt{\frac{N^2d^2(1-\theta^2)}{2\lambda}\left|\frac{1}{r}-\frac{1}{\bar{r}}\right|}$, and $C(\cdot)$ and $S(\cdot)$ denote the Fresnel functions written as $C(x)=\int_0^x \cos\left(\frac{\pi}{2}t^2\right)\mathrm{d}t$ and $S(x)=\int_0^x \sin\left(\frac{\pi}{2}t^2\right)\mathrm{d}t$, respectively. As the number of array antennas N approaches infinity, β also approaches infinity and f^{near} approaches zero.

The physical origin of this phenomenon is the variation in the wavefront curvature of EM waves at different propagation distances. As shown in Fig. 6, the correlation between the two array response vectors at different distances at the same angle approaches zero as the number of antennas increases.

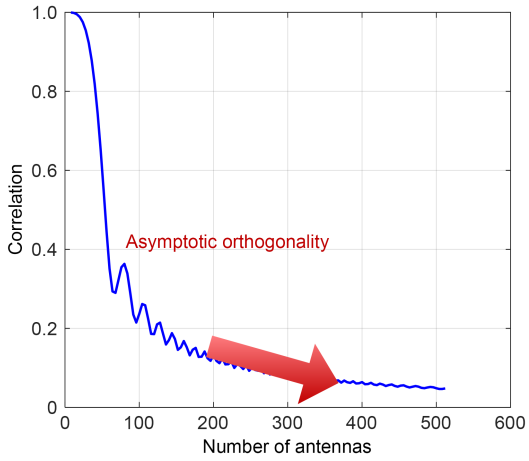

Fig. 6 Channel correlation versus antenna curve (Cui MY and Dai, 2022)

Based on Fig. 6, Cui MY and Dai (2022) analyzed the optimal sampling points at varying propagation distances for large-scale MIMO at the transmitter determined by wavefront curvatures. Results revealed that the optimal distance sampling in the near field is non-uniform due to wavefront curvature effects. Specifically, the optimal sampling points follow an inverse relationship (Cui MY and Dai, 2022):

$$r_s = \frac{C}{s}\left(1-\theta^2\right), \quad s = 1, 2, \cdots, \tag{3}$$

where C is a constant determined by the allowed coherence strength.

The two beam characteristics discussed above pertain to the ULA scenario, with further insights into the distance-domain focusing properties explored for uniform circular array (UCA) in the reference (Wu ZD et al., 2023). For UCA configurations, the beam focusing gain can be approximated by a zeroth-order Bessel function of the first kind. Comparative analysis showed that while ULA's beam focusing gain steadily decreases with reducing distance, UCA's beam focusing gain diminishes more rapidly. This difference suggests that UCA can concentrate signal power within a narrower range, thereby reducing power leakage.

2.3 Near-field performance analysis

2.3.1 Degree of freedom analysis

Using the Fourier plane-wave expansion channel modeling, Pizzo et al. (2022b) proposed a signal space methodology to analyze the DoFs of the EM fields under various scattering conditions, employing a Nyquist sampling perspective. This approach treats antenna elements as spatial sampling points and assesses the sampling point density required to reconstruct the EM field, which corresponds to the communication DoFs. Under isotropic propagation settings (Fig. 7), the number of spatial sampling points per square meter is reduced by 13% compared to conventional half-wavelength sampling. This reduction becomes increasingly significant with higher angular scattering selectivity, leading to a notable simplification.

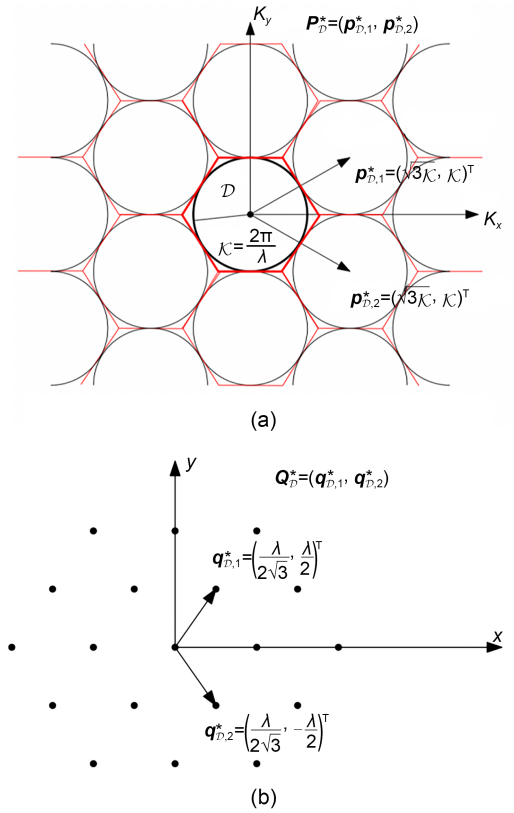

Fig. 7 Nyquist sampling under isotropic scattering conditions (Pizzo, 2020b): (a) circle packing in the wavenumber domain; (b) hexagonal sampling in the spatial domain

In related investigation, wavenumber domain modeling of near-field large-scale antenna arrays has revealed that the evanescent wave effect enhances the DoFs and communication capacity in near-field regions, demonstrating DoF gains of up to 30% in the typical reactive near-field region.

For spatially discrete-MIMO (SPD-MIMO) systems, a narrowband channel response matrix $\boldsymbol{H}$ yields the number of spatial DoFs of the channel corresponding to the count of positive singular values of $\boldsymbol{HH}$ or the rank of the correlation matrix $\boldsymbol{HH}^{\mathrm{H}}$. While far-field LoS conditions generally provide only one DoF, near-field spherical waves exhibit nonlinear phase shifts and varying power levels for each link, leading to increased diversity and a higher rank of the channel matrix. For a given aperture, the singular values of $\boldsymbol{H}$ display a characteristic two-slope pattern. Through simulations and measurements, it has been observed that for smaller values of N (where N is the number of transmit and receive antennas), the singular values of $\boldsymbol{H}$ gradually decrease followed by rapid decay beyond a critical threshold. This threshold defines the EDoFs, expressed as $\mathrm{tr}^2\left(\boldsymbol{HH}^{\mathrm{H}}\right)/\left\|\boldsymbol{HH}^{\mathrm{H}}\right\|_{\mathrm{F}}^2$ (Xie et al., 2023), and is illustrated in Fig. 8 (Ouyang et al., 2023). This phenomenon intensifies as the number of transceiver antennas increases because proximate antennas generate nearly indistinguishable receiver waves.

Furthermore, continuous-aperture arrays (CAPAs), known as CAP-MIMO, represent the limiting case of SPD-MIMO with infinite antennas. However, similar to SPD-MIMO, the singular values of the CAP-MIMO channel also exhibit a "two-slope" trend (Fig. 8). Therefore, in the near-field CAP-MIMO channel, performance remains constrained by the number of

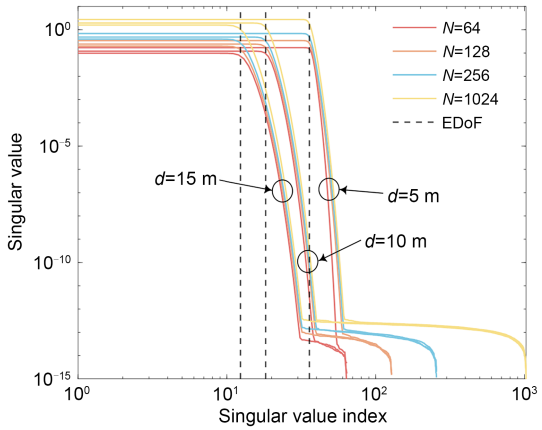

Fig. 8 Singular values of the near-field SPD-MIMO (Ouyang et al., 2023). Here, d denotes the transmission distance, and N is the number of transmit and receive antennas

EDoFs. To estimate the number of EDoFs in a near-field CAP-MIMO setup, the channel matrix $\boldsymbol{H}$ can be replaced with Green's functions (Xie et al., 2023). For CAPAs, the number of EDoFs is proportional to the product of the transmitter and receiver aperture areas and inversely proportional to the transmission distance (Ouyang et al., 2023).

2.3.2 Near-field performance analysis

The emergence of new physical characteristics in 6G near-field communications necessitates reevaluation of traditional performance analyses based on the far-field UPW model, such as asymptotic channel gains, within the framework of novel near-field models.

In traditional far-field models, the equivalent channel gain of a uniform planar array (UPA) demonstrates a linear or quadratic growth with increasing array size, eventually reaching infinity—a result that contradicts physical principles. To provide more comprehensive insights, new near-field spherical wave propagation models have been introduced by researchers, focusing on active (Lu HQ and Zeng, 2022; Dong and Zeng, 2022) and passive (Zheng BX and Zhang, 2022; Zheng BX et al., 2023) massive MIMO arrays. These models explore the asymptotic performance as the size of active/passive arrays approaches infinity. For near-field communications based on spherical waves, the equivalent channel gain grows nonlinearly as the number of active antennas or passive elements increases, introducing a novel angular span parameter (Lu HQ and Zeng, 2021). With infinite active antennas or passive elements, the equivalent channel gain stabilizes at a constant value (Dong and Zeng, 2022; Lu HQ and Zeng, 2022; Zheng BX and Zhang, 2022; Zheng BX et al., 2023; Zhuo et al., 2024). Unlike collocated massive MIMO arrays, sparse massive antenna arrays have a larger physical aperture, emphasizing their near-field properties. Wang HZ and Zeng (2023) demonstrated that spatial angle non-uniformities in sparse antenna arrays enhance interference suppression and spatial localization. In near-field MIMO, a larger array aperture expands the near-field communication region, enhancing spatial multiplexing gain due to spherical wavefront. Li XR et al. (2022) derived a closed-form expression of the near-field EDoFs at the bottom of this page.

In Eq. (4), η denotes the sparsity of the antenna array, l is the distance between the transmitter and the receiver, and $\overline{N}$ and $\underline{N}$ denote the maximum and minimum values of the number of transmit and receive antennas, respectively. Fig. 9 shows that the EDoF grows with increasing array sparsity until an upper limit is reached, defining a theoretical threshold for the optimal antenna sparsity at which the EDoF attains its maximum.

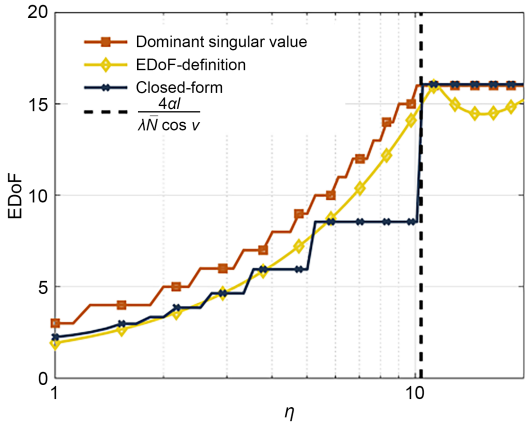

Fig. 9 EDoF versus array sparsity for sparse MIMO near-field communication systems (Wang HZ et al., 2024b)

A pioneering modular array design tailored for accommodating extremely large arrays has been explored (Li XR et al., 2022, 2023a, 2023b, 2024), known as the modular extremely large-scale array (XL-array), where elements were systematically arranged in a modular configuration on a shared platform. A near-field NUSW model for the modular XL-array

$$\varepsilon(\eta)\approx\begin{cases}1, & \eta<\dfrac{4l}{\lambda\bar{N}(\underline{N}-1)\cos v},\\ \dfrac{\underline{N}^2}{-\left\lfloor\dfrac{4\alpha l}{\lambda\bar{N}\eta\cos v}\right\rfloor^2+(2\underline{N}-1)\left\lfloor\dfrac{4\alpha l}{\lambda\bar{N}\eta\cos v}\right\rfloor+\underline{N}}, & \dfrac{4l}{\lambda\bar{N}(\underline{N}-1)\cos v}\le\eta<\dfrac{4\alpha l}{\lambda\bar{N}\cos v},\\ \underline{N}, & \eta\ge\dfrac{4\alpha l}{\lambda\bar{N}\cos v}.\end{cases}\tag{4}$$

was introduced (Li XR et al., 2022, 2023a), along with the development of closed-form expressions for near-field SNR. This analysis unveils the SNR scaling law and the system asymptotic performance. This work was extended (Li XR et al., 2023b, 2024) to explore modular XL-arrays' potential for improving the spatial resolution and potential communication performance.

In contrast to large-scale active antenna arrays, passive RISs are more likely to achieve extremely large-scale implementations owing to their cost effectiveness and low energy consumption. In passive RIS-based beamforming design, the beamforming gain provided by massive intelligent reflector arrays under the near-field model no longer follows the conventional "square-law growth" pattern (Wu QQ and Zhang, 2019). Instead, the gain stabilizes at a constant value as the number of reflective units approaches infinity (Zheng BX and Zhang, 2022; Feng C et al., 2023).

Beyond near-field communications, the deployment of extremely large-scale MIMO (XL-MIMO) systems shows promise in high-precision sensing, owing to their ultra-high spatial resolution. Near-field sensing benefiting from practical scaling laws offers advantages over conventional far-field models (Wang HZ and Zeng, 2022). A closed-form expression for the received SNR in near-field sensing was derived (Wang HZ and Zeng, 2022). Unlike the conventional UPW model, where the SNR scales linearly and unboundedly with the number of antennas, SNR in the near-field sensing increases with diminishing returns (Fig. 10).

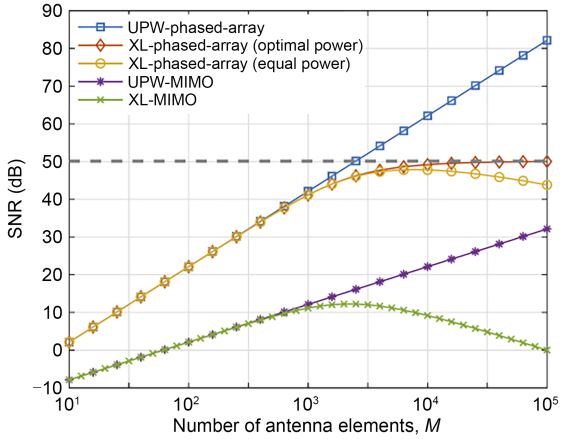

Fig. 10 SNR versus the number of transmit and receive antennas with the conventional UPW and the proposed models (Wang HZ and Zeng, 2022)

Furthermore, closed-form expressions for CRB for angle and distance parameters (Wang HZ et al., 2024a) in monostatic and bistatic near-field sensing systems were derived, focusing on XL-MIMO radar and XL-phased array radar. The Fisher information matrix for this is expressed as

$$\boldsymbol{F}=\frac{2}{N_0}\Re\left\{\left(\frac{\partial \boldsymbol{w}}{\partial \boldsymbol{z}}\right)\left(\frac{\partial \boldsymbol{w}}{\partial \boldsymbol{z}}\right)^{\mathrm{H}}\right\}, \tag{5}$$

where $\boldsymbol{w}$ is the output of the matched filter, $\boldsymbol{z}$ represents the parameter to be estimated, and N_0 is the noise power spectral density. Therefore, the CRBs for the angle and range, represented as $\boldsymbol{F}_{1,1}^{-1}$ and $\boldsymbol{F}_{2,2}^{-1}$ respectively, exhibit diminishing returns as the number of antennas increases, eventually approaching certain limits (Wang HZ et al., 2024a):

$$\begin{cases}\lim\limits_{\frac{D_{\mathrm{T}}}{r\cos\theta}\to\infty}\mathrm{CRB}_{\theta}=\dfrac{1}{2\gamma L}\dfrac{\lambda^2 d_{\mathrm{T}}\sin^2\theta}{8\pi^3 r^3\cos\theta},\\ \lim\limits_{\frac{D_{\mathrm{T}}}{r\cos\theta}\to\infty}\mathrm{CRB}_{r}=\dfrac{1}{2\gamma L}\dfrac{\lambda^2 d_{\mathrm{T}}\cos\theta}{8\pi^3 r},\end{cases} \tag{6}$$

where γ is the receive SNR, d_{T} is the transmit antenna element spacing, and λ is the signal wavelength.

Fig. 11 shows CRB for angle in monostatic near-field XL-MIMO and XL-phased array radar. The figure demonstrates that as the number of antennas increases, using an inappropriate far-field model to analyze near-field sensing with XL-arrays may result in significant errors. Further, the CRBs for the angle in the phased-array radar mode are smaller than those in the MIMO radar mode, as the former typically benefit from an additional transmit beamforming gain.

From an EM viewpoint, recent studies by Pizzo, Marzetta, and others provide methods to characterize the communication channel for a near-field massive antenna array within the wavenumber domain (Pizzo, 2020a, 2020b, 2022a). The core concept involves reconstructing the holographic MIMO (HMIMO) channel through Fourier expansion, modeling it with a finite set of sampling points in the wavenumber domain (Fig. 12). The spatial and wavenumber domains are also connected via the Fourier transform, allowing spatial domain channel modeling from the wavenumber domain channel:

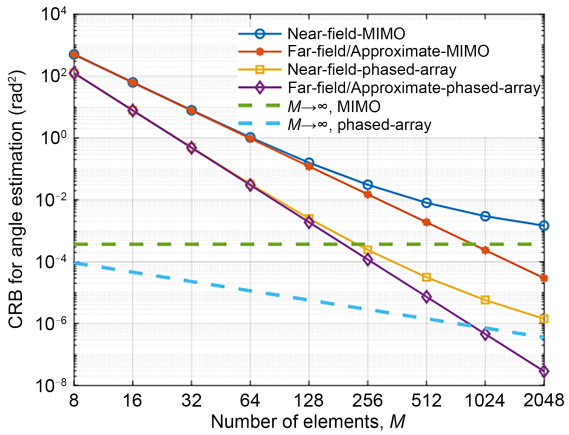

Fig. 11 CRB of angle for monostatic sensing

$$h(\boldsymbol{r},\boldsymbol{s})=\frac{1}{(2\pi)^2}\iiiint a_{\mathrm{r}}(\boldsymbol{k},\boldsymbol{r})\cdot H_{\mathrm{a}}\left(k_x,k_y,\kappa_x,\kappa_y\right)a_{\mathrm{s}}(\boldsymbol{\kappa},\boldsymbol{s})\,\mathrm{d}k_x\mathrm{d}k_y\mathrm{d}\kappa_x\mathrm{d}\kappa_y, \tag{7}$$

where $H_{\mathrm{a}}(k_x, k_y, \kappa_x, \kappa_y)$ denotes the wavenumber domain channel, $a_{\mathrm{r}}(\boldsymbol{k}, \boldsymbol{r})$ represents the receive wave vector, $a_{\mathrm{s}}(\boldsymbol{\kappa}, \boldsymbol{s})$ denotes the transmit wave vector, and $h(\boldsymbol{r}, \boldsymbol{s})$ is the spatial domain channel. The channel model consists of three main components: the transmit and receive wave vectors and the wavenumber domain channel.

Zhi et al. (2024) further explored the theoretical capacity limits of near-field communications in EM propagation channels. Based on Maxwell's equations and the Helmholtz wave equation, the study formulated an EM near-field channel model using Green's functions for extremely large-scale discrete arrays with single-polarized antennas. In single-user settings, a closed-form expression for the channel capacity based on the MRC detector was presented, revealing its asymptotic performance. The conventional Rayleigh distance was also revised to account for EM propagation channels. For multi-user scenarios, the study leveraged non-stationary attributes derived from the single-user case to propose two low-complexity, dominant-subarray-based linear precoding strategies. These schemes made use of visibility region (VR) and incorporated graph theory methodologies, reducing computational overhead.

Gong et al. (2023c) offered a comprehensive overview of the fundamental principles and technologies underlying HMIMO arrays for near-field communications (Fig. 13). The study examined both software and hardware components, aiming to provide a holistic understanding of the principles, technological advancements, and developmental trajectories in the field of HMIMO near-field communication.

3 Near-field channel models and channel measurements

For developing and evaluating near-field MIMO systems and technologies, realistic and straightforward channel models are essential (Gao HQ et al., 2023; Liu YM et al., 2024; Wang H et al., 2024; Zhang JH et al., 2024b). Various approaches to MIMO channel

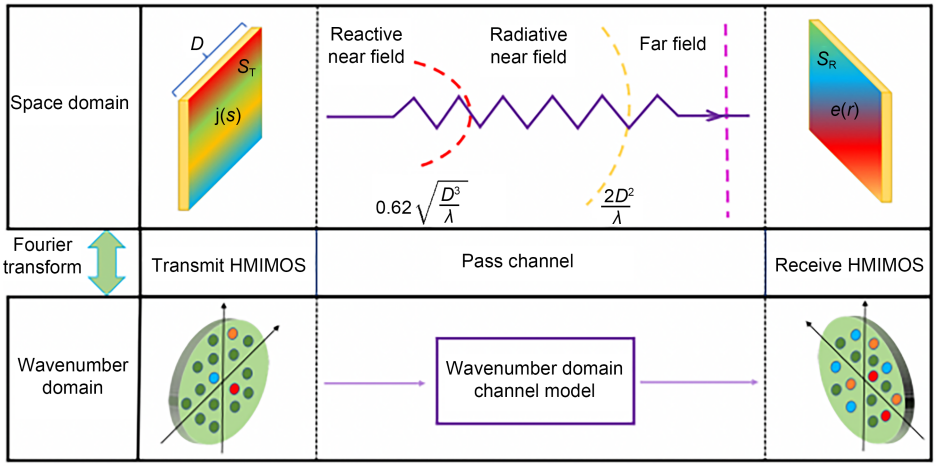

Fig. 12 Fourier plane-wave expansion channel model

Fig. 13 HMIMO communication application scenarios (Gong et al., 2023c)

modeling exist, based on different underlying principles, including statistical, deterministic, and EM-based models. As previously mentioned, unlike those of traditional small-scale antenna array systems, near-field MIMO channels exhibit distinct near-field propagation and SnS characteristics.

3.1 Near-field channel model

Deterministic channel models aim to accurately represent wireless channels by considering the physical environment and factors influencing signal propagation. Based on approximations of Maxwell's equations, these models calculate the EM propagation within the channel to offer highly spatially resolved insights into the signal behavior at specific locations. They are customizable to specific scenarios, making them valuable for understanding signal propagation mechanisms and optimizing system design. In contrast, statistical channel models describe wireless channel behaviors through statistical properties derived from extensive measurements. Statistical models lack site-specific precision and require large-scale measurements for parameter distributions. Additionally, they struggle to consistently adapt to dynamic environments. Statistical models are well-suited for large-scale network simulations and scenarios where detailed channel information is unnecessary, while deterministic models excel in precision-demanding environments such as mmWave communications, massive MIMO systems, and mission-critical communications where detailed spatial information is essential.

3.1.1 Statistical channel model

Numerous statistical channel modeling studies address the near-field characteristics. For instance, the Third Generation Partnership Project (3GPP) TR 38.901 standardized channel model (ETSI, 2020) recommends a spherical wave propagation to characterize near-field channels, assuming that signals radiate as spherical wavefronts from point sources. This approximation has been validated as more accurate and effective than the plane-wave approximation in near-field scenarios (Haneda et al., 2006), and thus it is widely used.

Despite this, few models address SnS properties for near-field MIMO systems (Zhang P et al., 2018). The COST 2100 model (Liu LF et al., 2012) first introduced the concept of VR to characterize SnS channels for MIMO antennas, later extended to massive MIMO antenna arrays (Zhang JH et al., 2017). VR confines the cluster activity to limited spatial areas, making clusters visible only to antenna elements within this region. In addition, visibility gain was introduced to capture the distance-dependent variation in cluster power across elements in VR. Several models based on VR were developed using the birth–death process

along the array axis to characterize the SnS property. Numerical analysis of statistical properties, such as correlation, quasi-stationarity regions, and average cluster lifetimes on the elements, was performed for model validation.

A near-field MIMO channel model integrating both near-field and SnS properties was proposed (Yuan ZQ et al., 2023a). This model effectively reveals SnS characteristics from the perspective of multipath propagation mechanisms. In addition, the model was experimentally validated with high accuracy in reconstructing the near-field SnS channel. A 3GPP-like channel simulation framework incorporating this model was proposed (Gao TY et al., 2023), highlighting its potential for future standardized modeling.

The model in Yuan ZQ et al. (2023a) is detailed as follows: assume K paths between the transmission (Tx) array and reception (Rx) in the scenario depicted in Fig. 14. The near-field MIMO channel at frequency f is modeled as a superposition of channel frequency responses (CFRs) of the K paths on the array as

$$\boldsymbol{H}^{\mathrm{sns}}(f)=\boldsymbol{S}\odot\boldsymbol{A}(f)\boldsymbol{H}(f), \tag{8}$$

where $\boldsymbol{H}^{\mathrm{sns}}(f)$ comprises M complex values, i.e., $\boldsymbol{H}^{\mathrm{sns}}(f)\in\mathbb{C}^{M\times 1}$, $f\in[f_{\mathrm{L}}, f_{\mathrm{U}}]$ denotes the frequency within the designed range, and $\odot$ represents the element-wise product operation. $\boldsymbol{H}(f)\in\mathbb{C}^{K\times 1}$ denotes CFRs of the K paths at the reference point (Fig. 14), expressed as

$$\boldsymbol{H}(f)=[\alpha_1 \mathrm{e}^{-\mathrm{j}2\pi f\tau_1}, \alpha_2 \mathrm{e}^{-\mathrm{j}2\pi f\tau_2}, ..., \alpha_K \mathrm{e}^{-\mathrm{j}2\pi f\tau_K}]^{\mathrm{T}}, \tag{9}$$

where α_k and τ_k (k=1, 2, ..., K) represent the complex amplitude and propagation delay of the k^{th} path, respectively, and $(\,)^{\mathrm{T}}$ denotes the transpose operation. $\boldsymbol{A}(f)\in\mathbb{C}^{M\times K}$ is the array manifold matrix. The array manifold projected onto the m^{th} antenna element by the k^{th} path, i.e., the matrix entry $a_{m,k}$, can be represented by the transfer difference of the m^{th} element with respect to the reference point:

$$a_{m,k}(f)=\frac{\|\boldsymbol{d}_k\|}{\|\boldsymbol{d}_{m,k}\|}\exp\left(-\mathrm{j}2\pi f\frac{\|\boldsymbol{d}_{m,k}\|-\|\boldsymbol{d}_k\|}{c}\right), \tag{10}$$

where c is the light speed, and $\|\ \|$ represents the Euclidean norm of the argument. $\boldsymbol{d}_k$ denotes the vector pointing from the reference point to the first scattering source of the k^{th} path propagation route, specifically:

$$\boldsymbol{d}_k=d_k[\sin\theta_k\cos\phi_k, \sin\theta_k\sin\phi_k, \cos\theta_k], \tag{11}$$

where d_k is the distance between the source and the reference point, and θ_k and ϕ_k denote the elevation and azimuth angles of the k^{th} path, respectively. $\boldsymbol{d}_{m,k}$ denotes the vector pointing from the m^{th} antenna element to the source point, and is formalized as

$$\boldsymbol{d}_{m,k}=\boldsymbol{d}_k-\boldsymbol{d}_m, \tag{12}$$

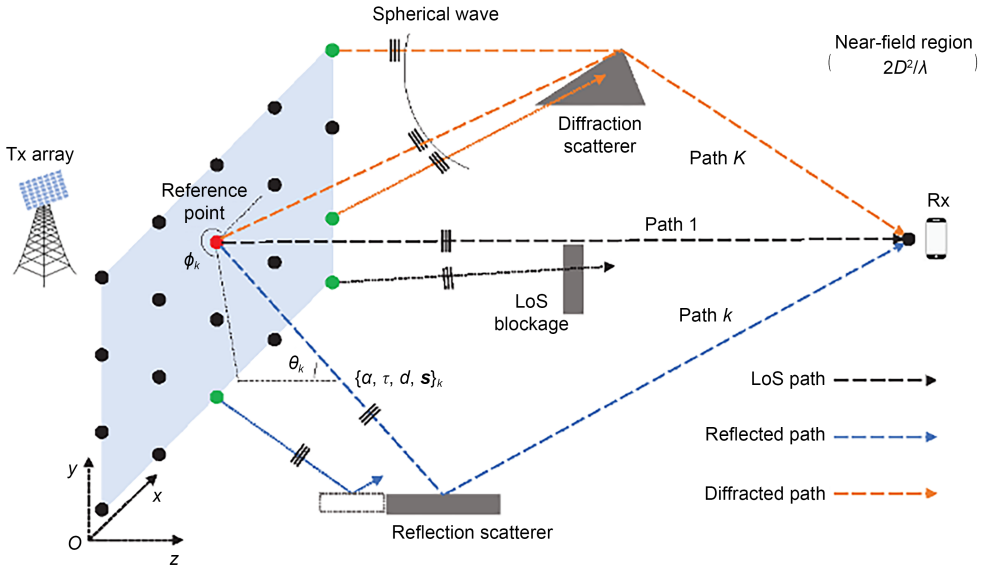

Fig. 14 Spherical propagation with the SnS property in the near-field MIMO channel (Yuan ZQ et al., 2023a)

where $\boldsymbol{d}_m$ is the position vector of the m^{th} element relative to the reference point.

The matrix $\boldsymbol{S}$ in Eq. (8) was introduced to characterize the SnS property. It contains K non-negative real-valued vectors:

$$\boldsymbol{S}=[\boldsymbol{s}_1,\boldsymbol{s}_2,\cdots,\boldsymbol{s}_K], \tag{13}$$

where $\boldsymbol{s}_k=[s_{1,k}, s_{2,k}, \cdots, s_{M,k}]^{\mathrm{T}}$ and $s_{m,k}$ (m=1, 2, ..., M) characterizes the SnS property of the k^{th} path on the m^{th} element. The model is also applicable to stationary channels by setting $s_{m,k}$=1 for m=1, 2, $\cdots$, M. Essentially, $\boldsymbol{S}$ denotes the SnS contributions of the paths on the antenna array. Different propagation mechanisms, such as stationary propagation, LoS blockage, incomplete reflection, and diffraction, result in varying SnS contributions. The value of the parameter $s_{m,k}$ is determined by the power distribution across these mechanisms. Denoting VR_k as the VR for the k^{th} path (i.e., elements in VR_k can view the k^{th} path, while those out of VR_k cannot), then $s_{m,k}$ reads as follows:

$$s_{m,k}\begin{cases}=0, & m\notin \mathrm{VR}_k,\\ =1, & m\in \mathrm{VR}_k \,\&\, \text{blockage/reflection},\\ \in(0,1), & m\in \mathrm{VR}_k \,\&\, \text{diffraction}.\end{cases} \tag{14}$$

Compared to existing VR-based models, the proposed model successfully reveals the SnS property, allowing for realistic and accurate reconstruction of both near-field and SnS phenomena (Yuan ZQ et al., 2023a). In terms of complexity, the model introduces only one additional parameter, s, to capture the SnS effect, compared to the conventional stationary modeling framework. Furthermore, the simplicity of this model enables flexible implementation. Specifically, customized near-field SnS channels under various conditions, such as stationary or non-stationary environments, dominant paths (i.e., LoS and reflected paths), or all paths, can be simulated in a laboratory setting by adjusting the SnS parameter.

3.1.2 Deterministic channel model

Deterministic channel models generally generate channels by reconstructing environments and calculating EM propagation. Among them, ray-tracing (RT) models are widely used for their high accuracy and relatively low complexity compared to full-wave EM calculations. RT can simulate the physical propagation of the channel between spatial locations, such as transmitter and receiver, with high precision, especially at high frequencies (Fuschini et al., 2019).

Conventionally, RT performs simple point-to-point simulations to predict the entire channel between Tx and Rx (Karstensen et al., 2016). However, this is insufficient for near-field MIMO channels as elements in such large arrays experience different sub-channels. A brute-force RT simulation, where each element pair between the Tx and Rx arrays undergoes separate calculations, is technically feasible but computationally prohibitive. Alternatively, various studies have developed more efficient RT-based multi-antenna channels. In Raschkowski et al. (2015), the METIS project (Mobile and Wireless Communications Enablers for the Twenty-Twenty (2020) Information Society) proposed a simplified RT simulation for massive MIMO systems, although no results were presented. In Ng et al. (2007), efficient multi-antenna RT simulations were introduced by incorporating acceleration strategies such as object space partitioning and grid computing. RT simulations for MIMO and massive MIMO systems were performed (Han C et al., 2015; Tan et al., 2015; Zhang Z et al., 2023), with comparisons to measurement data. However, these studies still relied on brute-force RT simulations for all element pairs. To improve efficiency, a plane-wave extension method was proposed (Yamada et al., 2009) within the RT framework for MIMO channel simulation, where the sub-channel of one Tx–Rx element pair was simulated using RT, and other sub-channels were obtained by expanding the RT-simulated sub-channel using plane-wave expansion under the far-field assumption, which is for MIMO radios with a small aperture.

State-of-the-art plane-wave extension method is widely adopted for MIMO systems with small-scale arrays. However, it becomes problematic for large-scale near-field MIMO system, as it fails to capture the crucial near-field and SnS effects. In Yuan ZQ et al. (2024), an accurate and efficient deterministic RT framework for near-field MIMO systems, known as the coarse-refinement method, was proposed. This method was designed to capture near-field and SnS properties. Essentially, it relies on RT simulations for a selected number of sparsely located array elements and

employs techniques such as spherical/astigmatic-wave approximations and non-stationary modeling to extend the RT-generated channels to the entire array. This method has been experimentally validated, demonstrating significant computational savings without sacrificing accuracy.

In the coarse-refinement method, the array is first divided into several groups. RT simulations are performed only for endpoints of each group to generate sub-channels. Based on these results, multipaths are classified into stationary and non-stationary along the group element axis. The elements visible for each path are determined as follows: (1) Stationary multipaths, meaning that paths are present at all endpoints in RT simulations and are directly reconstructed for all other elements within the group. All group elements are visible to these paths and will have a corresponding path response. (2) Non-stationary multipaths, which are not present at all endpoints of the group and require individual assessment to determine their presence on each element. The visible elements for these paths are identified during this process. Fig. 15 illustrates the coarse RT simulation process in the coarse-refinement method. As shown, two paths generated in RT at both ends are directly reconstructed for other elements, while the LoS path is individually determined for each element since it is present only at one group endpoint.

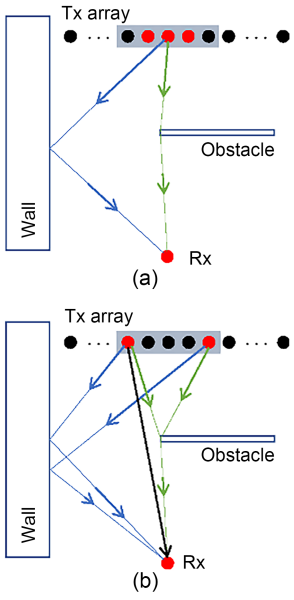

Fig. 15 Illustration of the coarse RT simulation process on a group for stationary and non-stationary paths (Yuan ZQ et al., 2024): (a) path generation for coarsely spaced elements (i.e., both ends); (b) path construction for visible elements

After defining path visibility for each element, the path responses are generated in the refinement process. Due to image propagation, paths undergoing LoS transmission or reflections correspond to spherical waves centered at the Rx or its image, i.e., virtual Rx (VRx). In contrast, diffraction alters wave shape; hence, paths undergoing one or more diffractions are captured as astigmatic-wave propagation. Fig. 16 illustrates the spherical/astigmatic-wave approximation for different propagation mechanisms, and the detailed extension equations in the refinement process can be found in Yuan ZQ et al. (2024).

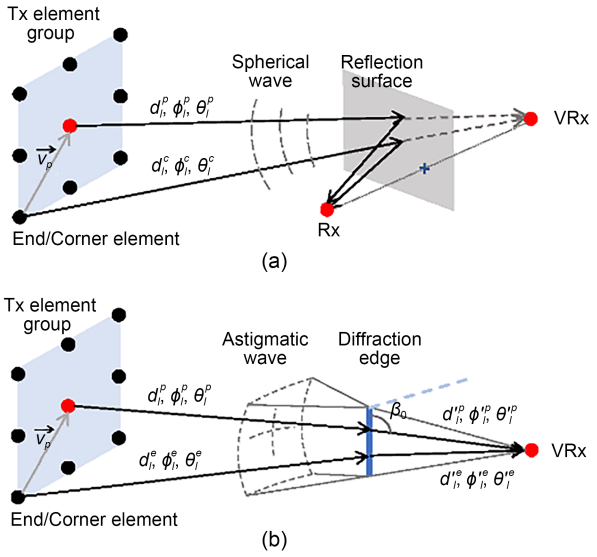

Fig. 16 Illustration of the refinement process with spherical/astigmatic-wave approximation (Yuan ZQ et al., 2024): (a) LoS transmission and reflection; (b) diffraction

The proposed method achieved accuracy close to the brute-force RT method but with significantly reduced complexity by simulating only a subset of array elements. By incorporating spherical/astigmatic-wave interpolation and non-stationary modeling, the method accurately characterized near-field propagation and SnS, avoiding any loss in precision. In contrast, the default extension method relied on linear interpolation of path parameters generated at the group ends. However, simple linear interpolation overlooks important factors such as path geometry, array distribution, and group non-stationarity, leading to potential accuracy degradation. Another default assumption is to ignore the

non-stationarity, treating the channel as a stationary near-field channel, which can cause significant inaccuracies in non-stationary channel realizations. These results highlight the importance of spherical/astigmatic-wave interpolation and non-stationary modeling for accurately reconstructing the near-field SnS channel. Despite the underlying principles being complex, their implementation does not significantly increase computational complexity compared to the RT simulations. In summary, the proposed method efficiently and accurately models the near-field MIMO channel while capturing near-field and SnS properties.

3.1.3 Challenges and potential solutions in applying the above-mentioned channel models

While deterministic and statistical channel models offer unique advantages in characterizing wireless channels, their application in real communication systems poses several challenges. Addressing these challenges is crucial to enhance the practical value of research in this field.

The challenges include:

1. Complexity vs. accuracy. Deterministic models, though detailed and accurate, often require intricate calculations based on physical principles, leading to higher computational demands. Statistical models are simpler to implement but may oversimplify channel characteristics, potentially overlooking subtle nuances crucial for accurate site-specific system design. Choosing the appropriate model depends on balancing complexity and accuracy to suit specific scenarios.

2. Dynamic environments. Wireless channels are inherently dynamic, affected by mobility, environmental changes, and interference. Both deterministic and statistical models may struggle to rapidly and consistently adapt to these variations, impacting communication system reliability.

3. Data requirements. Statistical models rely on extensive measurements to accurately capture statistical properties, which can be challenging in scenarios where acquiring such data is impractical or costly. Deterministic models, on the contrary, demand detailed knowledge of the physical environment for precise channel characterization.

To address these challenges, several potential solutions can be considered:

1. Hybrid models. Combining deterministic and statistical approaches can harness the strengths of both. By integrating deterministic models for specific regions of interest with statistical models for broader coverage, it is possible to enhance the overall accuracy while managing computational complexity.

2. Machine learning integration. Incorporating machine learning algorithms to adapt channel models based on real-time data can improve the robustness of both deterministic and statistical models in dynamic environments. Machine learning can assist in predicting channel behavior and optimizing system performance.

3. Parameter estimation techniques. Developing efficient parameter estimation methods can address the data requirements of statistical models. By optimizing measurement strategies and employing advanced estimation algorithms, researchers can improve the accuracy of the statistical models while reducing the need for extensive data collection.

Recognizing and addressing these challenges with innovative solutions can enhance the practical relevance of deterministic and statistical channel models in real communication systems. Embracing advancements in modeling techniques and exploring interdisciplinary approaches will lead to more robust and adaptive wireless communication systems, tailored to meet the evolving demands of modern telecommunications.

3.1.4 Electromagnetic information theory (EIT) based channel model

EIT is an interdisciplinary field that integrates EM, signal processing, and information theory to develop physically consistent communication schemes for improved transmission and processing of information. In near-field communication scenarios, consider that the physical characteristics of EM waves is particularly important. This is because spherical wave propagation in such scenarios introduces nonlinear phase, SnS, energy focusing, and other physical effects that differ from those in traditional far-field communication. To accurately model the LoS and NLoS signal transmission processes in the near-field range, researchers must integrate EM theory, enabling rigorous analysis of the performance limits in near-field communication.

First, we summarize the EIT channel modeling methods for LoS scenarios (Wei et al., 2023) in Fig. 17. The study investigated a scenario where both the transmitter and receiver are equipped with HMIMO surfaces comprising compact sub-wavelength tri-polarization

patch antennas operating in the near-field regime. The authors modeled the near-field tri-polarization channel between the surfaces using the dyadic Green function. By segmenting the HMIMO surface into subareas, the aperture of a transmitter–receiver antenna pair operates in a traditional far-field communication scenario, allowing for mathematical simplifications of the channel expression using techniques such as Taylor expansion and the Fraunhofer approximation. However, the transmitter and receiver arrays remain within the LoS near-field communication range. Theoretical analysis of the spatial correlation in the near-field region reveals that spatial proximity and distance have opposing effects on the correlation.

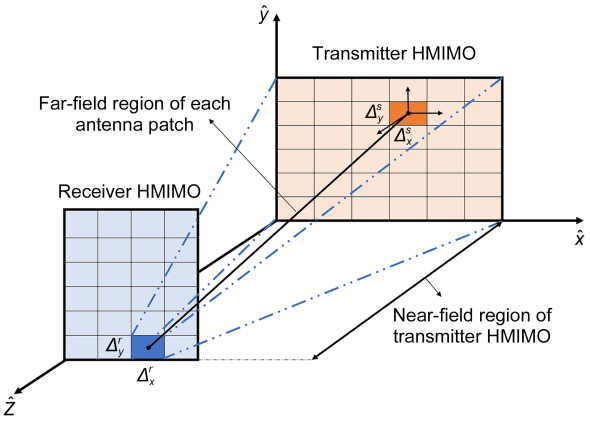

Fig. 17 HMIMO LoS communication (Wei et al., 2023)

Gong et al. (2023a, 2023b, 2023d) proposed a generalized EM domain near-field channel model for point-to-point HMIMO systems with arbitrarily placed surfaces in a LoS environment. Two computationally efficient channel models were developed from their integral counterparts, focusing on accuracy and conciseness. Furthermore, the capacity limits based on the proposed channel model were derived.

The spatial characteristics of near-field HMIMO channel were investigated (Björnson et al., 2021), revealing that it is possible to realize either a beam with finite depth and angular spread or a conventional angular beam with infinite focus in the radiative near-field of the HMIMO surface. The study derived the distance range where finite-depth beamforming is possible and where the near-field beamforming gain begins to taper off. Building on these near-field characteristics, Ramezani et al. (2023) investigated near-field channel modeling and two spatial multiplexing schemes in LoS communication scenarios: depth-domain multiplexing for multiple users and angular multiplexing for single-user data streams. The spatial multiplexing characteristics of different transmitter array architectures (e.g., fully digital, phase-shifters-based hybrid, and dynamic metasurface antenna (DMA) architectures) were extensively studied in Zhang HY et al. (2022).

Next, we address the EIT channel modeling methods for NLoS scenarios (Demir et al., 2022), extending multipath component modeling into the near field. In the far field, the channel is described as a discrete summation of plane waves arriving from different directions. However, in the radiative near field, the channel is expressed as a continuous summation of plane waves, which more accurately represents spherical waves. Specifically, the channel realization is determined by the angular spreading function.

Expanding the near-field channel model into plane waves, Pizzo et al. (2022a, 2022c) started with the Helmholtz equation of wave propagation and provided a Fourier plane-wave series expansion of the near-field channel using Wely's expansion. This approach captures the essence of EM propagation in arbitrary scattering environments. The expansion is based on Fourier spectral representation and has an intuitive physical interpretation, statistically describing the angular coupling between the source and the receiver. When discretized uniformly, this method yields a low-rank, semi-unitarily equivalent approximation of the EM channel in the angular domain. This channel model can be used to compute the near-field DoFs (Ji et al., 2023) and the ergodic capacity of point-to-point holographic MIMO systems with different degrees of CSI.

Another NLoS near-field channel modeling approach represents the channel as a superposition of spherical waves (Sherman, 1962; Cui MY and Dai, 2022). This method uses near-field steering vectors derived from an accurate spherical wave representation. Based on this near-field channel model, the energy spread effect in the angular domain was first identified, where a single near-field path component spread across multiple angles. To address this effect, polar-domain representations were introduced.

The information gain, measured by the number of spatial channels available for communication due to near-field and scattering effects, was investigated from an EM perspective (Franceschetti et al., 2015). It was revealed that information gain for EM fields is primarily a near-field effect. For the active power, this gain occurs only in the presence of scattering, where additional multiplexing capabilities arise, enabling the conversion of some reactive power into active power.

Considering the more general NUSW model, Dong and Zeng (2022) investigated the near-field channel model and spatial correlation for XL-arrays in NLoS scenarios. Unlike the far-field channel spatial correlation, which depends solely on the power angular spectrum, the near-field scattered power distribution is influenced by scatterers' angles and distances, resulting in a power location spectrum. An integral expression was derived for near-field channel correlation in terms of scatterers' location distribution, revealing that near-field channel correlation generally does not exhibit spatial stationarity.

In summary, we reviewed the most significant near-field channel models and introduced general models for LoS and NLoS communication scenarios. The EIT channel modeling methods are grounded in the EM propagation theory, such as the Helmholtz equation, Wely's expansion, and Green's function. By examining the relationship between excitation currents and the resulting electric fields of EM waves in different scenarios, these methods establish channel models that describe the spatial propagation of EM waves, ensuring physical consistency throughout the modeling process. Through EIT channel modeling, we have uncovered several new characteristics of near-field communication channels, including beam focusing, SnS, and nonlinear phase. These findings provide researchers with valuable insights for further exploring the channel capacity limits of practical physical channels and the performance limits of near-field communication systems.

3.2 Channel measurement in the near field

Measurement is the most fundamental and reliable method for obtaining realistic channel information. In the context of near-field MIMO channels, measurements reveal the differences and emerging features compared to traditional MIMO systems. Moreover, once these new characteristics are captured, channel measurement data continue to play an important role in guiding the modeling of near-field MIMO channels and in validating experimental results. Below, we summarize some representative studies on near-field MIMO channel measurements from literature.

In Payami and Tufvesson (2012), near-field MIMO channel measurements with two 128-element arrays at 2.6 and 3.5 GHz were performed to sound the channel. A virtual antenna array was formed by mechanically moving a single antenna to different spatial locations. This large array deployment enabled early observations of near-field propagation and SnS, and their impact on system performance was evaluated from the measurement data.

In Zhang JH et al. (2018), a large UPA consisting of 32–256 elements was used to detect near-field MIMO channel characteristics at 3.5 GHz. The study analyzed the statistical distributions of channel capacity and eigenvalue spreading. For mmWave bands, indoor measurements with 720- and 360-element virtual UCA were conducted (Zhang FC and Fan 2019; Cai et al., 2020; Yuan ZQ et al., 2023b). These studies explored parameter estimations for near-field channels, and effective estimation algorithms were proposed and experimentally validated. Near-field MIMO channel measurements at sub-THz and mid-band frequencies were conducted using directional virtual antenna arrays (Xu HX et al., 2024; Zhang JH et al., 2024a), capturing the effects of NF, SnS, and beam misalignment in THz channels. A sub-THz channel measurement with an omni-directional 2400-element virtual array at 100 GHz was conducted (Li MT et al., 2023; Yuan ZQ et al., 2023c; Zhang JH et al., 2024a), clearly capturing near-field and SnS characteristics from a multipath perspective. A 360-element sub-THz channel measurement at 100 GHz was conducted (Lyu et al., 2023), where beamforming technology—typically challenging at high frequencies due to incoherent phase measurements—was successfully implemented to extract channel multipaths from the array signals.

In addition, several near-field MIMO channel measurements were performed (Wang C et al., 2017; Wang Q et al., 2017; Li JZ et al., 2018), where space-alternating generalized expectation–maximization (SAGE) algorithms were applied for multipath parameter extraction,

and various scenarios—indoor and outdoor—were analyzed. Based on these measurements, it was concluded that two key assumptions of traditional MIMO systems may not hold in near-field MIMO systems due to near-field and SnS properties, namely the far-field plane-wave propagation and the spatial stationary assumptions.

In particular, as mentioned in Yuan ZQ et al. (2024), a 720-element near-field MIMO channel measurement was conducted to characterize the near-field and SnS properties, and a near-field MIMO channel model that realistically captures these effects was proposed. Fig. 18 illustrates the channels that were measured, simulated via brute-force RT implementation, and regenerated by the proposed statistical channel model. As shown, the measured channel paths were detected and marked with SnS phenomena, such as LoS blockage and power changes. The brute-force RT-simulated channel closely matches the measured channel, accurately reflecting near-field and SnS phenomena. Some mismatches arise due to simplifications in environment reconstruction. The proposed model successfully regenerates the channel, capturing the SnS observations with a high degree of similarity to the brute-force RT simulation.

Furthermore, as mentioned in Yuan ZQ et al. (2024), an efficient deterministic RT model, known as the coarse-refinement method, was proposed and validated through near-field MIMO measurements. Fig. 19 illustrates the channel responses from the measurement, brute-force RT simulation, and the

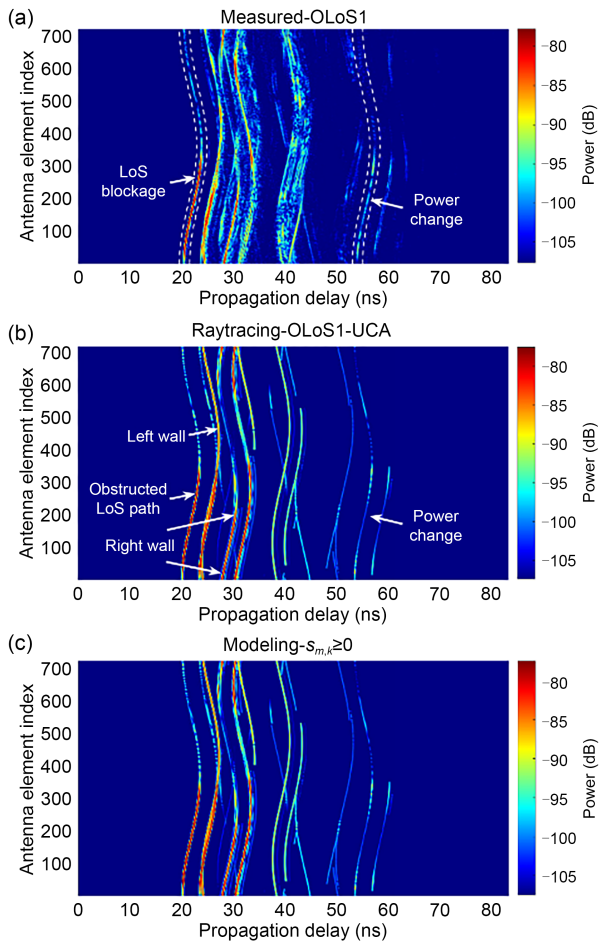

Fig. 18 Channel multipath responses from measurements and modeling in the obstructed-LoS1 (OLoS1) scenario (Yuan ZQ et al., 2024): (a) measured channel; (b) RT-simulated channel; (c) regenerated channel using the presented statistical model

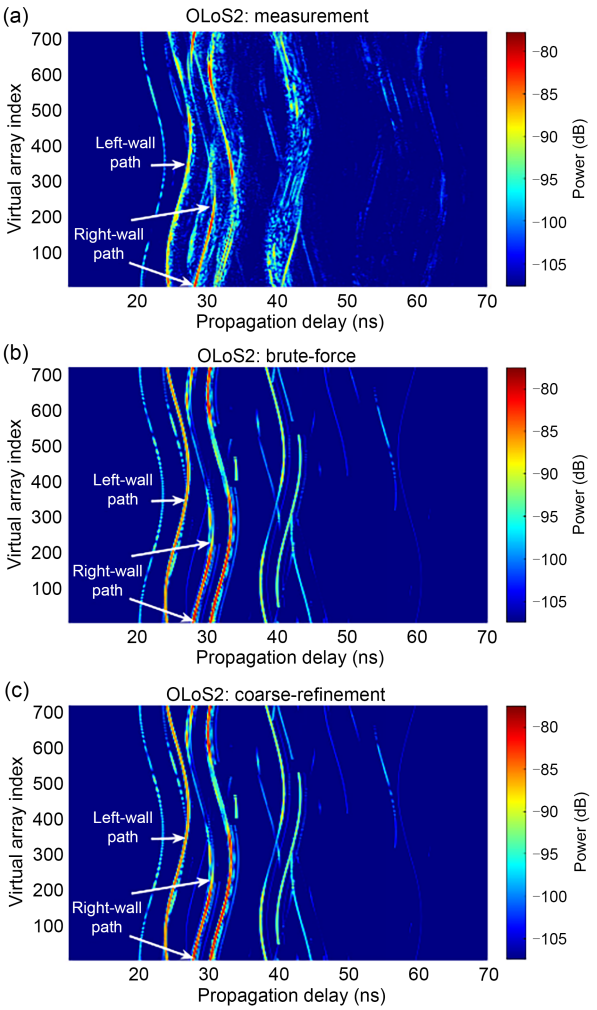

Fig. 19 Channel multipath responses from measurements and modeling in the OLoS2 scenario (Yuan ZQ et al., 2024): (a) measured channel; (b) RT-simulated channel by brute-force; (c) RT-simulated channel by coarse-refinement

coarse-refinement method. As shown, channel paths were detected and marked with SnS phenomena in the measurements, such as incomplete reflections from the right wall. The brute-force RT-simulated channel closely matches the measured channel, capturing both near-field and SnS phenomena, although some discrepancies arise due to environmental simplification. The proposed RT model is able to regenerate the channel with these SnS observations, achieving nearly the same modeling accuracy as the brute-force RT simulation while significantly reducing the simulation time by about 95%.

4 CSI acquisition for near-field communications

4.1 Channel estimation

Acquiring accurate CSI has always been essential for efficient beamforming and high-speed data transmission in MIMO communication systems. As the physical aperture of antenna arrays expands in upcoming 6G networks, the emerging near-field effects present new challenges in CSI acquisition. First, near-field MIMO systems typically incorporate a large number of antenna elements, significantly increasing the dimensionality of the channel to be estimated. Considering the limited number of radio frequency (RF) chains, the system would require an unacceptable pilot overhead if traditional least square (LS) estimator was used (Cui MY and Dai, 2022; Yu WT et al., 2023). Second, the far-field Fraunhofer approximation is no longer valid for modeling the near-field MIMO channels, necessitating the adoption of more sophisticated spherical wave models. This renders conventional far-field model-based estimation methods inaccurate. To address these challenges, new estimation methods should be designed to obtain CSI with low computational complexity and reduced pilot overhead. Table 1 presents a complexity analysis of several typical near-field channel estimation methods.

Recently, compressed sensing based estimation techniques have been extensively proposed to reduce pilot overhead and computational complexity in near-field MIMO channel estimation. Since near-field MIMO typically operates in mmWave or THz frequency bands, the channel exhibits a low-rank property due to the limited number of multipath components. This property can be exploited to acquire CSI reduced pilot overhead using compressed sensing algorithms.

For instance, a compressed sensing channel estimation algorithm for XL-MIMO was proposed (Cui MY and Dai, 2022), where a polar-domain near-field dictionary was designed to detect multipath components in the near-field region. In this region, the power diffusion effect can cause the detection of fake paths. To address this issue, a power-diffusion-aware orthogonal matching pursuit (OMP) channel estimation method was proposed to improve channel estimation accuracy (Yue et al., 2023). The spatial non-stationary issue in near-field MIMO was discussed (Han Y et al., 2020), where two OMP-based channel estimation methods, scatterer- and subarray-wise, were introduced. In Zhang X et al. (2024), a distance-parameterized angular-domain sparse model was presented for near-field MIMO channels, from which a joint dictionary learning and sparse recovery based channel estimation method was developed. To mitigate the beam squint problem in wideband MIMO communications, a frequency-selective polar-domain redundant dictionary was proposed in Li ZR et al. (2023) for wideband near-field MIMO channel estimation and localization. A parametric decomposition and compressed deconstruction framework was proposed in Chen YB et al. (2024), where the elevation angle, azimuth angle, and distance were estimated separately using variational Bayesian inference and message passing methods. A channel estimation method was introduced in Lu and Dai (2023) to address the mixed LoS/NLoS scenario, where the LoS path was modeled using the free-space propagation assumption, while the NLoS paths were based on the near-field array response vector. A strategy to determine whether MIMO operates in the near field, intermediate field, or far field was developed in Tarboush et al. (2024), along with a reduced dictionary based estimation algorithm designed to reduce computational complexity and improve estimation accuracy. Furthermore, Pan et al. (2023) proposed an algorithm for RIS-aided near-field joint channel estimation and localization (NF-JCEL) in THz systems. Based on a second-order Fresnel distance approximation of near-field channel characteristics, they designed a sampling Toeplitz covariance matrix to decouple distances and angles, estimating the horizontal and vertical AoAs of the UE, respectively. Finally, they estimated UE distances

Table 1 Complexity analysis of several typical near-field channel estimation methods

Reference	Algorithm	Complexity	Parameters
Cui MY and Dai (2022)	P-SIGW	$O\left(LPN_{\mathrm{RF}}NSM + N_{\mathrm{iter}}\left(P^2N_{\mathrm{RF}}^2M + PN_{\mathrm{RF}}M^2\right)\right)$	L: number of paths; P: pilot length; N_{RF}: number of RF chains; N: number of BS antennas; S: number of sampled distance rings; M: number of subcarriers; N_{iter}: number of iterations
Yu WT et al. (2023)	FPN-OAMP	$O\left(\log\left(\frac{1}{\varepsilon}\right)\left(4S^2\bar{S}Q+c\right)\right)$	ε: error tolerance; S: number of subarrays; $\bar{S}$: number of antenna elements of subarrays; Q: time slot; c: FLOPs of the neural network
Chen YB et al. (2024)	DDS-VBIMP	$O\left(N_{\mathrm{RF}}N_yN_z^2\right)$ per iteration	N_{RF}: number of RF chains; N_y: number of antenna elements along the y axis; N_z: number of antenna elements along the z axis
Zhang X et al. (2024)	DL-OMP	$O\left(3LK_{\mathrm{iter}}PN\right)$	L: number of paths; K_{iter}: number of iterations; P: pilot length; N: number of BS antennas
Lu Y and Dai (2023)	Two-stage CE algorithm	$O\left(\left(S_{\mathrm{LoS}}+MI\right)N_{\mathrm{RF}}N_1N_2\right) + O\left(N_1N_2\left(S_1+S_2\right)L\right)$	S_{LoS}: size of the parameter collection; N_{RF}: number of RF chains; N_1: number of Tx antennas; N_2: number of Rx antennas; S_1, S_2: number of grids; M: time slot; I: number of iterations; L: number of NLoS paths
Tarboush et al. (2024)	HSPWM-RD	$O\left(G_{\mathrm{ovs}}G_{\mathrm{T}}N_{\mathrm{L}}\left(N_{\mathrm{R}}-1\right)N_{\mathrm{T}}\right) + O\left(G_{\mathrm{ovs}}G_{\mathrm{R}}N_{\mathrm{L}}\left(N_{\mathrm{R}}-1\right)N_{\mathrm{T}}\right)$	G_{ovs}: oversampling factor; G_{T}, G_{R}: dictionary size; N_{L}: number of the dominant beamspace elements; N_{T}, N_{R}: number of Tx/Rx subarrays
Xiao J et al. (2023)	U-MLP	$O\left(N^3+N_{\mathrm{RIS}}S\right)$	N: number of BS antennas; N_{RIS}: number of RIS elements; S: number of samples
Ye et al. (2024)	IE-Pix2pix	$O\left(N_{\mathrm{T}}N_{\mathrm{R}}\left(N_{\mathrm{T}}+N_{\mathrm{R}}\right)\right) + O\left(\sum_{s=1}^{S}F_{s,\mathrm{h}}F_{s,\mathrm{w}}K_s^2N_sN_{s-1}\right)$	N_{T}: number of Tx antennas; N_{R}: number of Rx antennas; $F_{s,\mathrm{h}}$, $F_{s,\mathrm{w}}$: height and width of the output feature map respectively; K_s: filter size; N_s: number of output feature maps in the s^{th} layer
Li ZR et al. (2023)	CDL	$O\left(\varsigma\left(M_{\mathrm{NRIS}}+M_{\mathrm{RIS}}\right)N_{\mathrm{RF}}N^2LN_{\mathrm{S}}\right)$	ς: redundant rate; M_{NRIS}, M_{RIS}: pilot length; N_{RF}: number of RF chains; N: number of BS antennas; N_{S}: number of subcarriers; L: number of distance grids
Lei et al. (2024)	P-MRDN	$O\left(BMNQK^2E^2\right)$	B: number of ASPP-RDNs; M: number of layers of the RDN; N: number of BS antennas; Q: number of sampled grids; K: kernel size; E: number of features
Lei et al. (2024)	P-MSRDN	$O\left(B(M+4)NQK^2E^2\right)$	B: number of ASPP-RDNs; M: number of layers of the RDN; N: number of BS antennas; Q: number of sampled grids; K: kernel size; E: number of features

using one-dimensional searching and reconstructed the channel based on the near-field LoS channel model.

With the maturity and widespread adoption of artificial neural networks, methods using deep learning (DL) to assist in near-field MIMO channel estimation and reduce pilot overhead have garnered significant attention. DL-based methods can be categorized into two types: data-driven and model-driven. The former adopts pure neural networks to learn a direct mapping from received pilot signals to the estimated channel or its equivalent parameters, while the model-driven approach combines expert knowledge of wireless communications with neural techniques.

1. Data-driven DL channel estimation. Convolutional neural networks have been applied for near-field XL-MIMO channel estimation (Lee A et al., 2022). Multilayer perceptron neural networks have been used to estimate channels in MIMO systems with SnS (Xiao et al., 2023). Techniques like weight pruning and quantization were employed in Gao S et al. (2024) to accelerate the channel estimation process using

XL-MIMO channel network (XLCNet). Federated learning has also been used for mixed far- and near-field channel estimation, offering low overhead and privacy protection in cell-free communication systems.

2. Model-driven DL channel estimation. In Ye et al. (2024), a Pix2pix structure—a variant of the conditional generative adversarial network—was employed for channel estimation, where the generator network used an initially estimated channel as the input. The scarifying dictionary was formulated as a neural network layer and was embedded in the neural network for XL-array channel estimation in Zhang XY et al. (2023). A low-complexity, highly-adaptive fixed-point network for channel estimation was proposed in Yu WT et al. (2023). Inspired by the polar-domain channel transform, Lei et al. (2024) developed a residual dense network for channel estimation.

4.2 Beam training

By performing a beam search within a predesigned codebook, the objective of beam training is to identify the optimal codeword that best aligns with user's channel (Chen KJ et al., 2024). In conventional far-field beam training, only angular-domain beam search is necessary. However, near-field beam training must consider the angle and range domains, leading to significant time overhead with traditional exhaustive beam searches (Cui MY et al., 2023b). Therefore, low-overhead near-field beam training schemes are essential. To address this, DL-based near-field beam training schemes were proposed in Liu W et al. (2023a, 2023b). These schemes require only testing far-field wide-beam codewords, with the test results being fed into trained convolutional neural networks to map the best available near-field beams. Based on this DL-based scheme, additional tests using the probability vectors outputted by the neural network can further improve beam training performance. For cascaded channel scenarios involving RIS, Zhao (2024a) proposed a novel solution that employs a cascaded channel decoupling strategy. This approach simplifies the RIS regulation matrix by dividing the EM wave modulation process into two separate sub-processes, virtual reception response and virtual regulated transmission, thereby achieving decoupling of the RIS cascaded channel.

4.2.1 Two-stage beam training scheme

Near-field beam training requires capturing both the angle and range information of the user (Wu CY et al., 2024). The two-stage beam training scheme first acquires user's angular information and subsequently scans the range based on the obtained angle (Zhang S et al., 2024). In a conventional approach, beam search within the angular domain necessitates scanning each sampled angle, resulting in a considerably increased training overhead. To reduce this overhead, the beam search was designed in the angular domain as a hierarchical structure, as shown in Fig. 20. In this design, the angular information was searched layer by layer by generating beams with varying angular coverage. By employing only two codewords per layer, overhead in the angular domain was reduced to a logarithmic scale relative to the number of antennas (Zhang S et al., 2024). Once the beam search in the angular domain is complete, the range information is determined by using near-field beams corresponding to different distances at the obtained angle. The proposed two-stage beam training scheme is applicable to both phased array and reconfigurable holographic surface assisted communication systems (Zhang S et al., 2024).

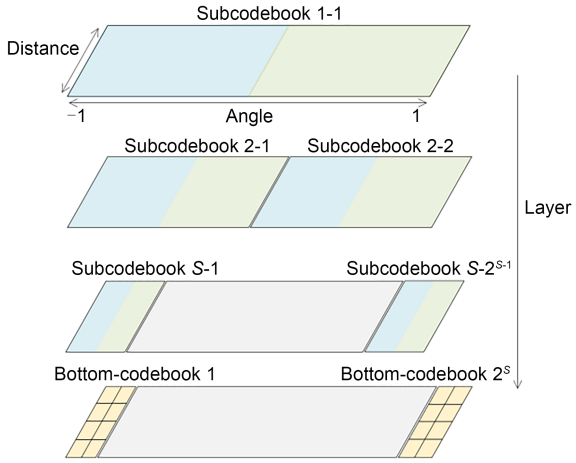

Fig. 20 Near-field two-stage beam training (Zhang S et al., 2024)

4.2.2 Multi-user simultaneous beam training scheme

Traditional beam training schemes require conducting a beam search for each user individually. When a large-scale array serves multiple users, the overall beam training overhead increases in proportion to the

number of users (Zhang YT et al., 2022). To reduce overhead in multi-user scenarios, it is crucial to design a beam training scheme that can serve all users simultaneously. In this context, a hierarchical simultaneous beam training mechanism was proposed, as shown in Fig. 21, where each layer consists of only two codewords (Zhang YT et al., 2023). These two codewords collectively cover the entire service area, each covering half. By designing the beam coverage in adjacent layers to follow a progressive relationship, both angle and distance information can be deduced from user feedback in each layer (Zhang YT et al., 2023).

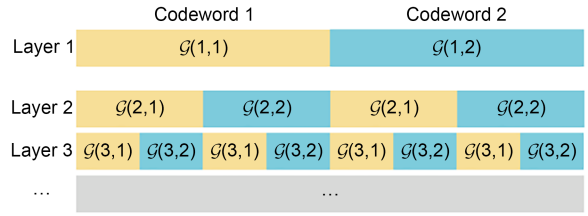

Fig. 21 Multi-user simultaneous beam training (Zhang YT et al., 2023)

Liu W et al. (2024a, 2024b) introduced DL-based near-field beam training schemes to alleviate the significant pilot overhead required in multi-user scenarios. A graph neural network (GNN) based near-field multi-user beam training scheme was proposed in Zhao YJ et al. (2019), where only far-field wide beams need to be tested for each user. The corresponding beamforming gain information was then mapped to the best available near-field codeword via the GNN. This GNN-based scheme further improved beam training accuracy by leveraging the position correlation between adjacent users. After determining each user's near-field codeword, a beam allocation scheme based on probability vectors was proposed to effectively mitigate beam conflicts (Liu W et al., 2024a). Inspired by the similarity between far-field sub-6 GHz channels and near-field mmWave channels, Liu W et al. (2024b) proposed to leverage sub-6 GHz uplink pilot signals to directly estimate the optimal near-field mmWave codeword. This approach reduces pilot overhead and bypasses traditional channel estimation. DL was employed to perform this dual mapping function—sub-6 GHz to mmWave, far-field to near-field—using a novel neural network structure called NMBEnet, which enhances the precision of beam training.

4.3 Codebook design

In wireless networks employing large-scale arrays, beamforming schemes that rely on accurate CSI require effective acquisition. However, implementing large-scale arrays establishes numerous links between the BS and users, leading to significant complexity in acquiring CSI (Shtaiwi et al., 2021). To address this challenge, researchers have introduced beamforming schemes based on codebook design and beam training. In these schemes, predefined codebook codewords were employed for beam training, and the optimal codeword that provided the highest received power for the user was selected for beamforming (Ning et al., 2020).

Given that the coverage of conventional small-scale antenna arrays predominantly encompasses the far field, codebooks were designed based on the far-field channel model. However, as antenna apertures increase, the near-field region also extends. As shown in Fig. 22, users are randomly distributed across both the near and far fields. Due to the different propagation characteristics of EM waves in these two regions, traditional far-field and near-field codebooks are no longer suitable for such hybrid near–far field scenarios (Zhang YT et al., 2022).

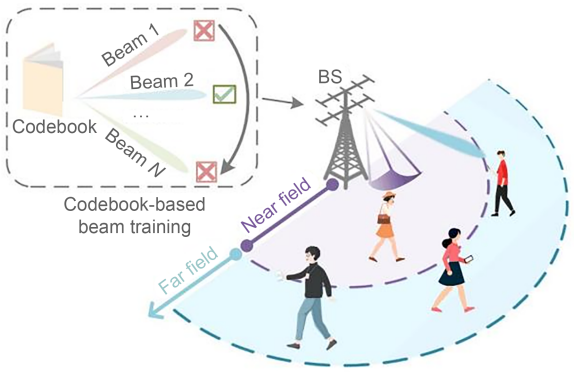

Fig. 22 Codebook-based near–far-field communications (Zhang YT et al., 2022)

To enable effective beamforming in this hybrid near–far field scenario without prior knowledge of user distribution, a codebook was desiged which considers the propagation properties of both near-field spherical waves and far-field plane waves (Zhang YT et al., 2023). Each codeword in the proposed codebook was designed to simultaneously cover the near

and far fields. The design process involves the following steps (Zhang SP et al., 2023):

Step 1: codebook coverage discretization. Transmitter's coverage was divided into near and far fields based on EM wave propagation characteristics. Unlike conventional boundaries like the Rayleigh distance, to avoid excessive division of the near-field region and redundant near-field codewords, an effective near–far field boundary was introduced. This boundary was defined as the range where the beamforming gain achieved using the spherical wave model closely aligns with that of the plane wave model.

Step 2: equivalent channel modeling. Using the characteristics of EM wave propagation, equivalent channels from the transmitter to each discretized area were established.

Step 3: codeword design. Codewords were designed based on the principle that the received signal power within codeword's coverage remains constant, while outside the coverage, the received signal power diminishes to zero. By applying this principle to the equivalent channels, a closed-form solution for each codeword can be derived.

As shown in Fig. 23, the following schemes are compared: (1) traditional far/near field codebooks and (2) perfect CSI. The results show that with the same number of codewords, the proposed near–far field codebook achieves a higher sum rate than the pure far-field codebook and an impressive enhancement over the near-field codebook. Moreover, its performance approaches that of the perfect CSI case.

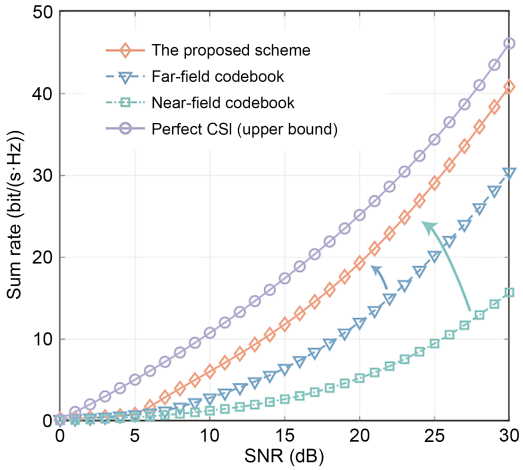

Fig. 23 Sum rate vs. SNR with different codebooks (Zhang SP et al., 2023)

5 Near-field beams

5.1 General discussion on near-field beams

In MIMO communication systems, beamforming is crucial for enabling high-speed transmissions in high-frequency bands such as mmWave and THz frequencies. Conventional far-field beamforming steers the radiated signal energy toward a specific angle. In contrast, near-field beamforming focuses on the radiated signal energy on a specific location, determined by the angle and distance. This is why near-field beamforming is referred to as beam focusing. Beam focusing allows energy to be concentrated over a range of distances, providing additional resolution in the distance dimension, which presents both opportunities and challenges for near-field communications (Cui MY et al., 2023a).

In terms of opportunities, the extra distance-focusing ability of near-field beams opens new possibilities for enhancing spectral efficiency. In Björnson et al. (2021), the concept of DF defined as the region with high beamforming gain was rigorously analyzed. The DF indicates that high beamforming gain could be achieved only within a certain distance window, quantitatively characterizing the distance-focusing ability of near-field beams. Leveraging this property, near-field narrowband multi-user MIMO communication was explored, where optimization-based beamforming algorithms were applied in fully digital, hybrid precoding DMA systems (Zhang HY et al., 2022). Moreover, in far-field communication systems, spatial division multiple access (SDMA) has been fundamental to multi-user MIMO communications. In contrast to the far-field SDMA, where only the angle domain is harnessed to enable multiple accesses, the concept of location division multiple access (LDMA) was proposed in Wu ZD et al. (2023), where the additional distance-focusing ability was used to mitigate inter-user interference. In LDMA, near-field channels become asymptotically orthogonal as the number of antennas increases, enabling multiple users to be served simultaneously. In addition, UCA was proposed to expand the near-field region over wider angles compared to the common ULA, allowing more users to benefit from near-field communications (Wu ZD et al., 2023).

In terms of challenges, the model mismatch between far-field UPW-based beamforming and near-field NUSW environment leads to inaccurate beamforming when using conventional far-field methods (Cui MY et al., 2023a). To compensate for this performance loss, near-field beamforming methods have been investigated, particularly in narrowband systems (Björnson et al., 2021). In wideband scenarios, the misfocus effect was first identified in Myers and Heath (2022), where the mismatch between far-field UPW and near-field NUSW causes beam misfocus in the distance domain. To address this, an optimization-based method was proposed to retrieve the beamforming loss. A bandwidth continues to increase, and the near-field beam split effect becomes evident in XL-MIMO systems. In Cui MY and Dai (2024), a piecewise far-field model was introduced to approximate the near-field model. This method partitions the entire antenna array into several subarrays, where the user could be considered in the far field of each subarray. In this way, time-delay units could be employed to eliminate the near-field beam-split effect, significantly enhancing spectrum efficiency in wideband XL-MIMO systems. For XL-MIMO near-field beam design, reducing computational complexity and improving real-time performance are key challenges. To address these, AI technologies have been employed for near-field beam design. An online learning framework was proposed to optimize analog phase shifts (Zhang Y and Alkhateeb 2023), while deep reinforcement learning was used to design wideband hybrid analog-and-digital beam focusing by selecting codewords from a predesigned near-field codebook. In practice, far-field and near-field users typically coexist in the communication area, making mixed-field communication a critical area of study (Han C et al., 2024). To address this, a proximal policy optimization based mixed-field beam design algorithm was proposed to serve far-field and near-field users effectively.

The modeling of near-field communication primarily relies on the free-space Green function to establish an EM channel model. However, this free-space model may not accurately reflect real-world scenarios where EM waves propagate primarily along the ground. To address this issue, Jiang YH and Gao (2023) established a basic EM framework for half-space MIMO wireless communication. The study analyzed the EDoF for discrete and continuous-aperture MIMO systems in a half-space environment, showing that in near-field communication, the difference between half-space EDoF and free-space EDoF is significant and should not be overlooked.

Another key feature of near-field transmission is its ability to support high-rank transmission, which can effectively improve the EDoF of the channel, by multiplexing multiple signals on the same spatio-temporal-frequency resources. This enables multi-stream signal transmission without requiring multipath propagation, enhancing transmission robustness and rate and effectively supporting future applications such as augmented reality (AR) and virtual reality (VR).

5.2 Non-diffractive beams

There are two main types of EM wave convergence for near-field antennas. One is to gather the radiated EM wave energy at a focus point called near-field focusing. The other is to gather the radiated EM wave energy along a strip to maintain diffraction-free propagation called near-field beamforming, also known as non-diffractive beamforming. Non-diffractive beamforming avoids the limited energy convergence area associated with near-field focusing, allowing the signal to be maintained over longer distances and effectively extending the transmission range. It also offers new features, such as self-healing, enabling transmission around obstacles, making it a promising technology for future 6G applications. In this subsection, we will analyze typical non-diffractive beams, including Bessel and Airy beams, and explore their propagation properties and advantageous use cases.

5.2.1 Near-field-enabled Bessel beams

To accommodate the diverse application scenarios of 6G networks and meet their varying requirements, it is essential to design appropriate precoding strategies tailored to different transmission objectives. The near-field channel introduces new DoFs, making the need for flexible and adaptive precoding design more critical. Personalized and scenario-specific precoding designs will be the key to realizing the wide-ranging functionalities of 6G networks.

In near-field focusing applications, the focal spot is typically small, resulting in a limited coverage area. This limitation becomes more pronounced as the array

size increases, since it requires more precise alignment and tracking of the target user, significantly increasing the complexity of maintaining effective communication. Additionally, the small size of the focal spot presents challenges in supporting mobility. In scenarios where the target user or device is in continuous motion, the near-field focusing system must quickly and accurately adjust the focal point, demanding high tracking capability and processing speed, particularly in high-speed environments like communication for high-speed trains or cars.

Specifically, the radial coverage of a near-field focused beam is very limited. This limitation can lead to issues such as slower CSI updates, channel estimation errors, and delayed beam switching, all of which can significantly impact the quality of service for users. In high-speed mobility scenarios, for instance, the rapid changes in user position require higher tracking accuracy and faster response to ensure the stability and reliability of the communication link. These challenges necessitate advanced technologies and algorithms to achieve precise positioning and rapid beam adjustment, thus meeting the high-performance demands of 6G networks across diverse scenarios.

To enhance SNR of the received signals, expand coverage, and better support user mobility, high-frequency near-field beamforming solutions offer significant potential. Among them, Bessel beams (Khonina et al., 2020) stand out due to their unique non-diffractive properties and stable axial intensity distribution. The non-diffractive nature of Bessel beams allows them to maintain a stable intensity distribution during propagation, making them particularly effective in scenarios that require stable signal transmission.

Bessel beams can be viewed as a superposition of plane waves covering all azimuth angles from 0° to 360°, forming a specific angle ϕ_c with the propagation axis, known as the convergence angle of the Bessel beam. The implementation of Bessel beams relies on LoS near-field channels, and the corresponding precoding must precisely match the characteristics of these channels to ensure beam's formation and stable transmission. The precoding can be expressed as $\phi_2(n, n)=\exp(\mathrm{j}kl\sin\phi_c)$, where l represents the distance between the n^{th} element and the center of the transmitter. This beamforming precoding achieves a conical wavefront through phase compensation.

According to the characteristics of the zeroth-order Bessel beam, the depth of field—defined as the length of non-diffractive region—and the half-power bandwidth (HPBW) (Ettorre et al., 2018) are

$$\begin{cases} z_{\max}=\dfrac{D}{2\tan\phi_c(f)}, \\ \mathrm{HPBW}=\dfrac{2.235\lambda}{2\pi\sin\phi_c(f)}. \end{cases} \tag{15}$$

In practical applications, increasing the convergence angle enhances the beam focusing ability but limits capacity to maintain focus over longer distances, which can be problematic for scenarios requiring long-distance stable transmission. Conversely, decreasing the convergence angle extends the non-diffractive region, allowing the beam to remain stable over greater distances, but this also increases cross-polarization components, thereby affecting signal purity and transmission quality. Therefore, in designing non-diffractive beams, it is essential to balance the convergence angle, DF, and cross-polarization effects to meet the requirements of various application scenarios.

Fig. 24 shows the intensity distribution of a Bessel beam generated under a transmission frequency of 30 GHz, using a transmitter with 60×60 units and a convergence angle $\phi_c=8\arcsin(\lambda/(4D))$. In the figure, λ represents the wavelength and D represents the transmitter aperture. There is a significant deviation between the beam obtained with 1-bit quantization and the target beam. However, simulation comparisons reveal that the beam shape is significantly optimized when using 2-bit quantization.

In the direction of signal propagation, Bessel beams generated through conical wavefront phase design exhibit excellent non-diffractive characteristics. Within the designated propagation range, these beamforming techniques achieve a uniform energy distribution, offering a more consistent energy distribution compared to near-field focusing beams. This feature of Bessel beams ensures high signal stability and continuous coverage, even in scenarios involving user mobility. The stable non-diffractive nature of these beams is particularly crucial for wireless communication systems in dynamic environments. In high-frequency near-field communication applications, such as those

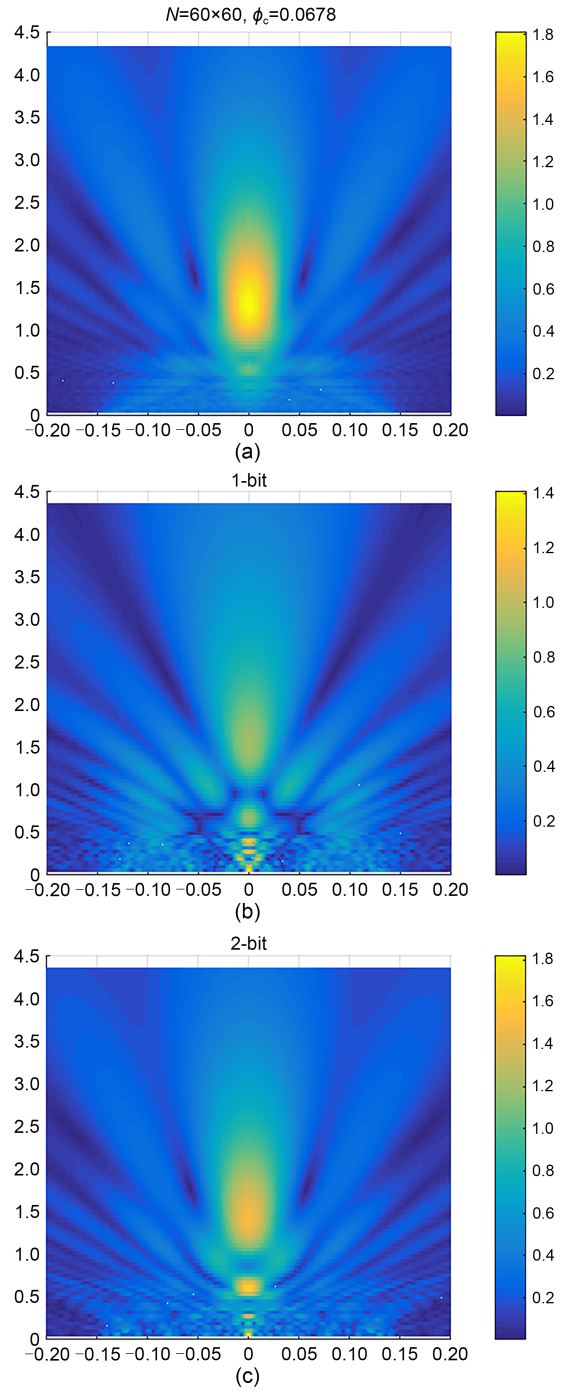

Fig. 24 Bessel beam intensity distribution and the impact of quantization: (a) Bessel beam; (b) 1-bit Bessel beam; (c) 2-bit Bessel beam

found in 5G and 6G networks, Bessel beams effectively address signal instability caused by high-speed movement, providing a robust solution for maintaining communication continuity and reliability. As a result, Bessel beams hold significant potential for future high-speed wireless communication technologies, especially in scenarios demanding high stability and continuous coverage.

For high-order Bessel beams, in addition to their non-diffractive properties, they possess the characteristics of non-diffractive vortex waves (Khonina et al., 2020; Li L et al., 2023). In addition, other non-diffraction beams, such as Airy and Pearcy beams, can be combined with vortex waves to exploit the orthogonality and diversity of OAM modes, offering richer functionality. In near-field scenarios, the research and application of vortex waves are more feasible than those in far-field scenarios. Bessel beams, with their non-diffractive characteristics, maintain a stable energy distribution during propagation. Even when partially obstructed, the central portion of the beam remains strong, ensuring signal integrity. This makes Bessel beams particularly suitable for high-density urban environments and industrial Internet of Things (IoT) scenarios, where they can effectively handle signal interruptions caused by small obstacles, ensuring stable communication links.

5.2.2 Airy beams

As a special self-bending beam, Airy beam possesses several unique physical characteristics. First, airy beams exhibit non-diffractive characteristics (Abdou, 2023). They resist significant spreading due to diffraction during propagation, maintaining high energy density and focus. This makes Airy beams highly promising for applications in imaging, sensing, and other fields. Furthermore, Airy beams exhibit self-acceleration characteristics (Zhou KZ et al., 2020), meaning that they can self-bend laterally during propagation. This allows them to bypass obstacles or achieve nonlinear propagation, offering unique advantages in signal transmission, target positioning, and energy transfer. In addition, Airy beams have self-healing capabilities; they can return to their original beam shape after being blocked by small objects. This feature enhances their robustness and stability in complex environments.

Compared to near-field focusing beamforming, the diffusion of Airy beams during propagation is significantly reduced, extending their effective propagation range and making them suitable for near-field wide-beam solutions. In addition, when the direct path

is blocked, the self-bending acceleration of Airy beams allows them to bypass obstacles and avoid transmission interruptions, a crucial feature for future high-frequency LoS transmission scenarios.

Although Bessel beams also exhibit non-traditional wavefront and propagation characteristics, they lack self-acceleration properties of Airy beams. Due to the special propagation characteristics of Airy beams, complex beamforming and diverse beam propagation paths can be achieved through the careful design of transmitters and beamforming parameters. This flexibility opens new possibilities for EM wave control, making Airy beams promising in a variety of applications, such as laser shaping, beamforming, and imaging.

With technological advancements, especially the application of metasurfaces, the generation and manipulation of Airy beams have become simpler and more efficient. Metasurfaces enable the creation and control of Airy beams more efficiently and compactly, overcoming the limitations of large optical systems traditionally required for generating Airy beams. In addition, the numerous units that compose metasurfaces allow precise control of Airy beam, enabling flexible adjustments to its shape, propagation direction, and energy distribution to suit various application needs. In Fig. 25, both theoretical and simulated beams based on Airy beamforming are shown. The generated wave clearly exhibits self-bending properties and effectively bypasses obstacles.

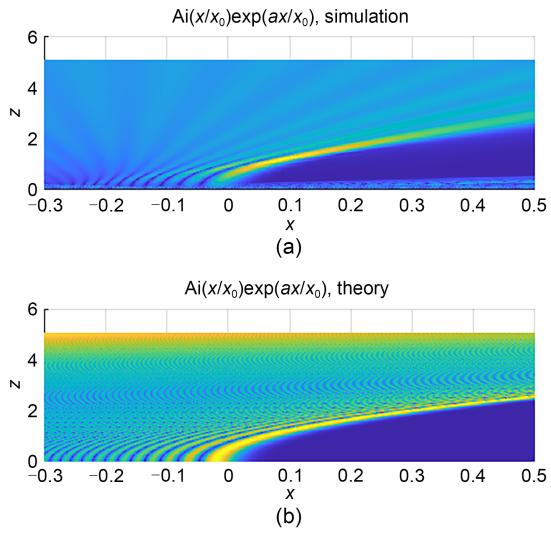

Fig. 25 Airy beams based on simulation (a) and theory (b)

Airy beams' curved propagation and self-healing characteristics allow them to bypass obstacles through phase modulation while maintaining signal integrity. In dynamic environments and high-speed scenarios, Airy beams can flexibly adjust their propagation paths, making them ideal for intelligent transportation, autonomous driving, and other complex applications requiring frequent obstacle avoidance.

5.3 Near-field-enabled OAM beams

This subsection explores OAM transmission in the near field, focusing on its hardware architecture and signal processing techniques (Yang et al, 2023). This study examines the design and implementation of OAM mode multiplexers, de-multiplexers, and antennas, along with the signal processing methods necessary for generating, detecting, and separating OAM modes.

5.3.1 Hardware architecture of the OAM system

The hardware architecture for data transmission based on vortex waves requires both the transmitter and receiver for system construction. In the theoretical expression of the vortex wave, the helical phase factor $e^{j/\Phi}$ is applied after the traditional plane wave. This spiral phase factor shows that vortex waves with different OAM modes can introduce a new orthogonal dimension, distinct from time, frequency, and polarization. Leveraging this mode orthogonality can significantly enhance system performance.

The spiral phase factor reflects that the classic UCA model can guide the design of hardware devices (Thidé et al., 2007; Mohammadi et al., 2010; Lin et al., 2017; Li L et al., 2018; Sasaki et al., 2018; Xue H et al., 2022b). The phase distribution in a UCA can be achieved using single antennas, antenna arrays, metasurfaces, spiral phase plates, etc., to implement the transmitter and receiver for vortex waves and complete the hardware system. Further optimization of the UCA model can be achieved through non-uniform circular array (NUCA), uniform elliptical array (UEA), and uniform concentric circular arrays (UCCAs) to adjust and enhance deflected beams, high-order OAM modes, and mixed modes. These optimizations facilitate the design of compact, multi-functional, and high-performance hardware devices (Sasaki et al., 2018). Due to the popularity of antennas

in modern wireless communication systems and their ability to manipulate OAM beams, UCCA- and metasurface-based OAM transmissions hold great potential.

UCCA-based systems represent a typical OAM hardware architecture, as shown in Fig. 26. This architecture integrates OAM and MIMO technologies, further enhancing the DoFs and multiplexing gain in OAM wireless transmission (Sasaki et al., 2018; Lee D et al., 2023). By incorporating MIMO technology, this design reduces the requirements for perfect alignment between the transmitter and receiver antennas, providing greater flexibility for the OAM receiver. This architecture can also be expanded to a UCAA- and/or UCCA-based OAM non-parallel misaligned transmission model and an off-axis misaligned point-to-multipoint OAM transmission model (Chen R et al., 2020), as shown in Fig. 27. By replacing the antenna array with metasurfaces and corresponding feeds, metasurface-based manipulation, transmission, and multiplexing of OAM signals can be achieved (Yu SX et al., 2016, 2017; Han JQ et al., 2018; Shuang et al., 2020; Long WX et al., 2021b; Feng Q et al., 2022). This allows for the direct multiplexing and demultiplexing of multi-channel signals, reducing the need for complex signal processing.

OAM design can be integrated with traditional beam control schemes using various hardware devices. By leveraging the frequency or polarization characteristics of the hardware, OAM can be combined with other EM dimensions to design linear polarization, circular polarization, and multi-frequency vortex waves. Simultaneous modulation of the same dimensional parameters at the transmitter and receiver can be achieved to complete the transmission of the beam (Liu Q et al., 2018; Xu P et al., 2023). Using tensor holographic metasurfaces, a single device can simultaneously and arbitrarily control both spin angular momentum (SAM) and OAM, using anisotropic properties (Xue H et al., 2023), as shown in Fig. 28. Active devices, such as pin diodes or varactor diodes, can be incorporated into the vortex wave hardware. By

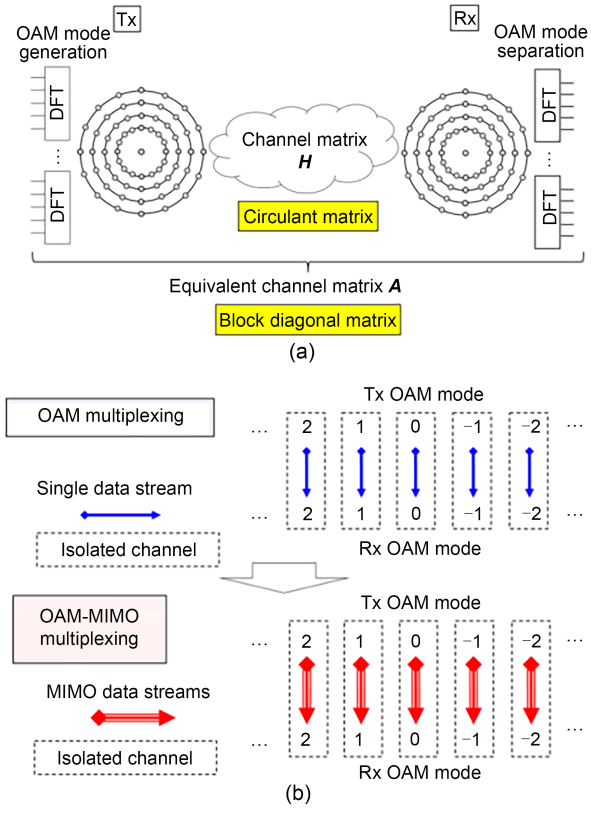

Fig. 26 UCCA-based OAM hardware architecture (Sasaki et al., 2018): (a) OAM-MIMO multiplexing system; (b) equivalent channel matrix of OAM and OAM-MIMO multiplexing

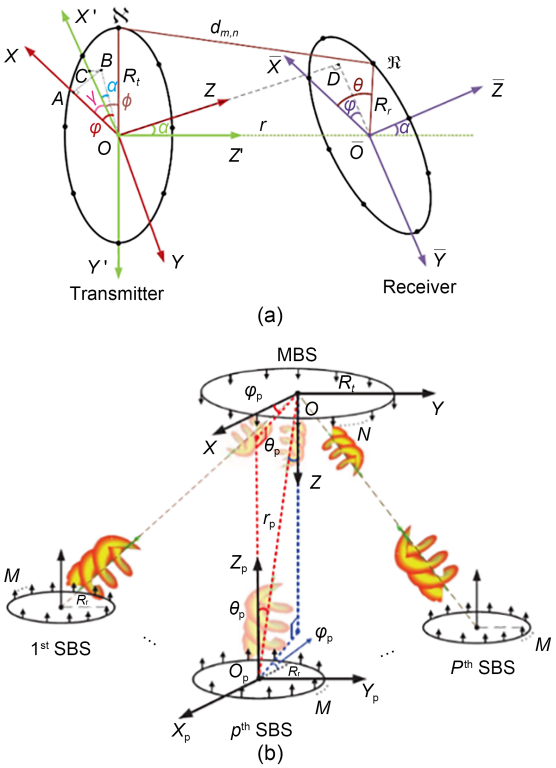

Fig. 27 UCA-based point-to-point (Chen R et al., 2020) (a) and point-to-multipoint (Long WX et al., 2021b) (b) OAM transmission structure

controlling these active components, reconfigurable antennas and metasurfaces enable real-time switching of the vortex wave's spatial propagation direction, OAM mode, and other beam states in the time domain, improving beam coverage and greatly expanding the range of the vortex wave applications.

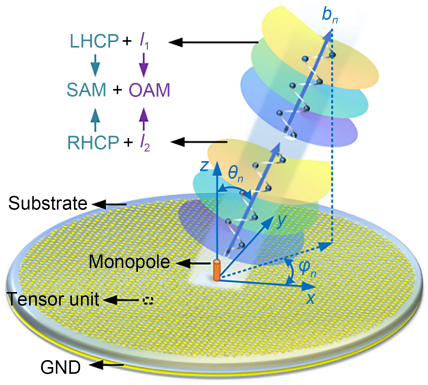

Fig. 28 Schematic of co-modulating of SAM states and OAM modes based on the anisotropic holographic metasurface (Xue et al., 2023)

In the near-field applications, vortex waves can be combined with non-diffractive beams, such as Bessel, Airy, Pearcy, and other special beams featuring unique properties. This combination offers enhanced performance, such as reducing the divergence characteristics of high-order vortex waves and providing a feasible solution for miniaturization and improved efficiency at the receiver (Kadlimatti and Parimi, 2019; Meng et al., 2020; Xue H et al., 2022a). Since these special beams often have unique initial field distributions, they demand greater amplitude and phase control capabilities from the beam generation device. On one hand, these beams can be generated through joint amplitude and phase modulation, and on the contrary, hardware design can be simplified by optimizing the functions corresponding to the special beams. For example, since higher-order Bessel beams inherently contain a spiral phase factor, Bessel vortex waves can be generated by superposing inward and outward conical waves, requiring only phase modulation from the hardware (Cui MY et al., 2023a). For circular Airy beams with circular symmetry, the helical phase factor can be loaded onto the beam, significantly reducing the amplitude variation requirements of the hardware through a truncated asymptotic function (Xue H et al., 2022a). The flexible modulation of EM waves via metasurfaces to achieve near-field vortex waves contributes significantly to miniaturized designs and simplified hardware architectures in near-field applications.

5.3.2 Signal processing of the OAM transmission

OAM wireless transmission continues to encounter numerous practical challenges, including designing the optimal topology for OAM transmission and reception to maximize channel capacity and developing low-complexity precoders and combiners for existing OAM architectures. The OAM index modulation (IM) method (Basar, 2018; Fan et al., 2021; Li N et al., 2023) and the OAM precoding and combining schemes (Chen R et al., 2020; Long WX et al., 2021b) offer potential solutions to these challenges.

The precoding scheme combining OAM with IM (Basar, 2018) not only transmits information symbols through conventional modulation on OAM beams but also conveys information via the combinations of activated OAM modes. At the OAM receiver, a back-propagation neural network was employed to precisely identify the activated OAM modes (Li N et al., 2023). This method achieves excellent spectral efficiency (SE) while maintaining low bit error rate (BER), offering an innovative strategy for precoding in UCA-based OAM wireless transmission.

In addition, UCA-based OAM structures can transmit OAM beams carrying information symbols, but this requires precise alignment between the transmitted and received OAM beams. Misalignment compromises the orthogonality between different OAM modes, leading to significant degradation in system's transmission performance. As indicated (Chen R et al., 2020; Long WX et al., 2021b), the channel characteristics of OAM wireless transmission are entirely determined by the relative positions of the transmitting and receiving UCAs. Therefore, accurately estimating these relative positions to obtain complete CSI is crucial for UCA-based OAM systems. To deal with this issue, a mode-frequency multi-time estimation-of-signal-parameters-using-rotational-invariance-techniques (M-F MT-ESPRIT) algorithm was proposed for point-to-point OAM scenarios (Long WX et al., 2021a). During the training phase, this algorithm processes received pilot samples multiple times across the frequency and OAM mode domains using the ESPRIT

algorithm to determine the relative distance and AoA between the transmitter and receiver, thereby providing complete and accurate CSI. A recursive ESPRIT algorithm for point-to-multipoint OAM scenarios was proposed in Long WX et al. (2023), specifically designed to estimate the AoAs of OAM beams transmitted by the macro base station (MBS) at the small base stations (SBSs). This recursive ESPRIT method differs from conventional ESPRIT algorithms by integrating the recursive characteristics of Bessel functions in UCA-based OAM signals, providing a potential method for obtaining the CSI in multi-user OAM systems.

After obtaining the AoAs using the recursive ESPRIT algorithm (Long WX et al., 2023) and determining the distances using fast Fourier transform (FFT), a null-space-based OAM precoding approach was proposed (Long WX et al., 2021b) for multi-user OAM systems. This method uses the estimated positions to design a beamforming matrix at the MBS, addressing inter-mode interference caused by OAM beam misalignment and co-mode interference originating from multiplexing the same OAM modes among different users. As shown in Fig. 29, the multi-user OAM system employing this precoding scheme achieves good BER performance, with an SE improvement of approximately 30% compared to conventional MIMO. More importantly, as illustrated in Fig. 30, the energy efficiency of this scheme is twice that of existing MIMO systems. Additionally, following the estimated positions, Chen R et al. (2020) proposed a low-complexity receive combining method. This solution first uses the estimated AoA to design a beam steering matrix to align the received OAM beams. Subsequently, a low-complexity amplitude combiner, based on the estimated distance, was proposed (Chen R et al., 2020) to accurately recover the information carried by the OAM beams. As shown in Fig. 31, this method incorporates the M-F MT-ESPRIT algorithm from Long WX et al. (2021a) and achieves strong BER performance while improving SE by approximately 20% compared to conventional MIMO transmission.

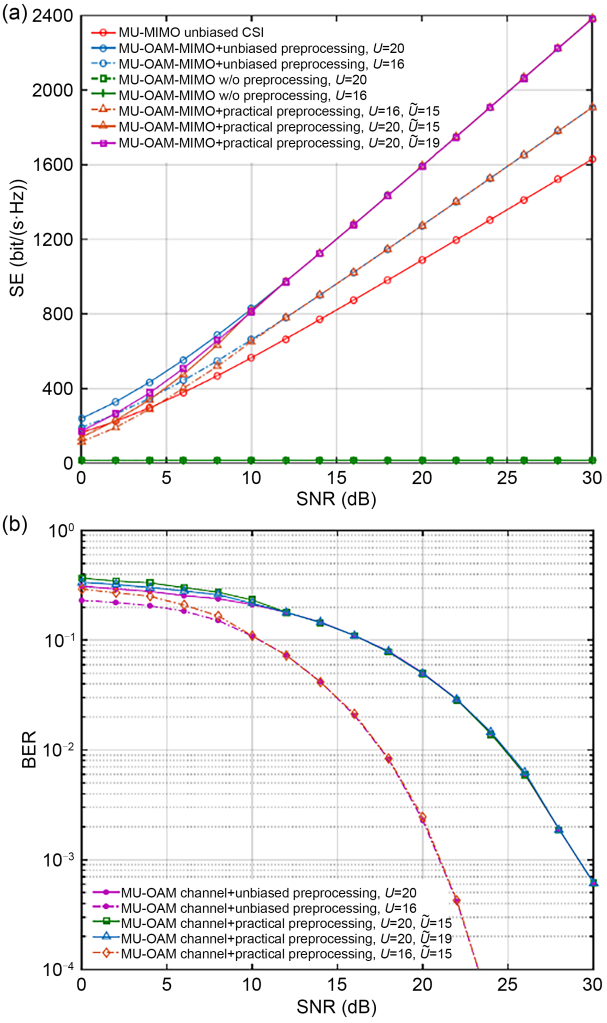

Fig. 29 Spectral efficiency (SE) vs. SNR for the UCCA-based point-to-multipoint OAM transmission (a) and BER vs. SNR for the UCA-based point-to-multipoint OAM transmission (b) (Long WX et al., 2021b)

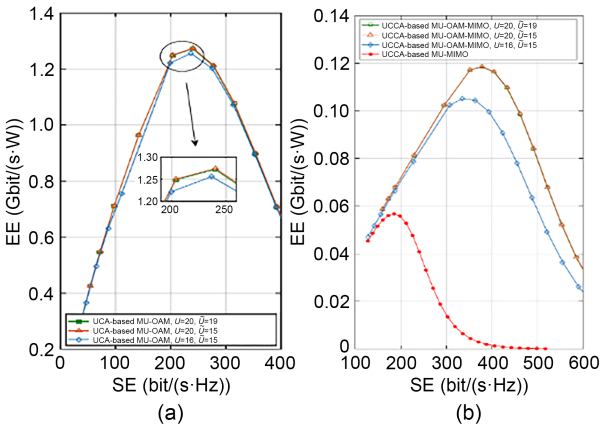

Fig. 30 Energy efficiency (EE) vs. SE for the UCA-based (a) and UCCA-based (b) point-to-multipoint OAM transmission and conventional MIMO transmission (Long WX et al., 2021b)

5.4 Secure beam focusing design

In future wireless networks, many applications will involve the exchange of sensitive information, making it crucial to ensure transmission security against

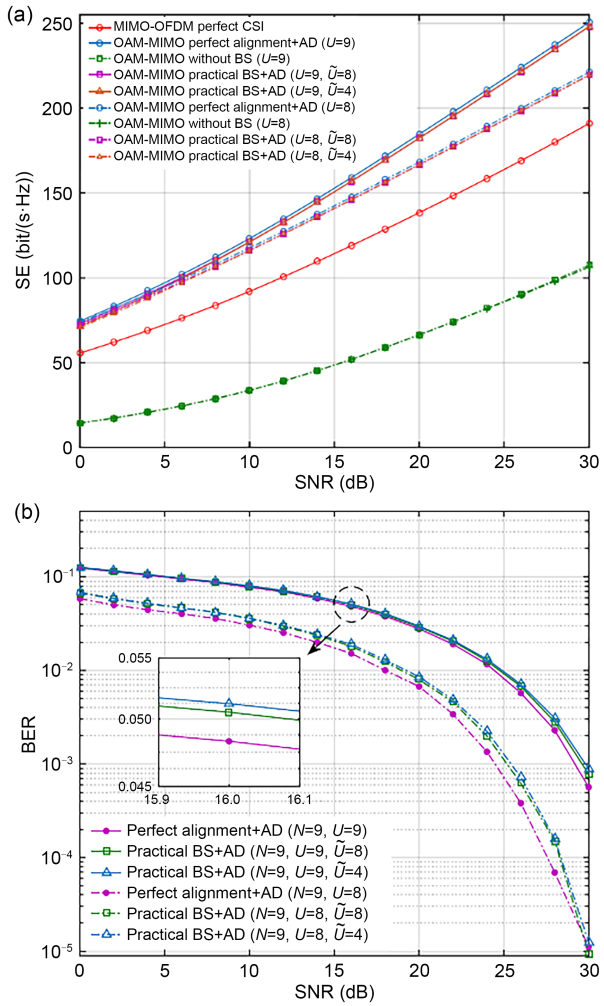

Fig. 31 Spectral efficiency (SE) vs. SNR for the UCCA-based point-to-point OAM transmission (a) and BER vs. SNR for the UCA-based point-to-point OAM transmission (b) (Long WX et al., 2021b)

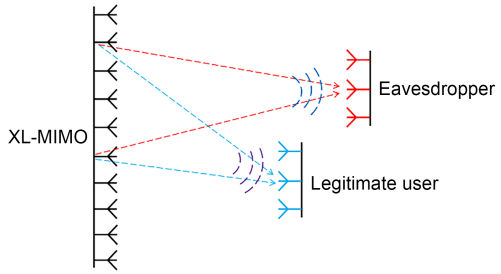

Fig. 32 Secure beam focusing design for near-field communication systems

malicious attacks such as eavesdropping and jamming. As shown in Fig. 32, near-field communications provide an additional DoF in the distance domain, enabling secure beam focusing designs.

A hybrid beamforming strategy has been developed to enhance near-field security (Zhang Z et al., 2024). A two-stage algorithm was designed to obtain the optimal beamformers that maximize the near-field secrecy capacity. This research reveals that the near-field security is more dependent on distance disparity than on angular disparity. An extremely large-scale RIS (XL-RIS) empowered near-field physical layer security communication system was considered to counter jamming and eavesdropping attacks in Cui Z et al. (2024), where the beamformer, artificial noise, and XL-RIS reflection coefficients were jointly designed. Additionally, an XL-RIS-empowered system was explored for enabling covert communications from Alice to Bob while evading detection by Willie (Liu J et al., 2024). This work demonstrated that near-field covert communications can achieve higher rates than far-field scenarios, even when Willie is positioned closer to the XL-RIS than Bob. Furthermore, some studies have investigated physical layer security for near-field wideband communication systems. A true-time delayed hybrid beam focusing architecture was designed to mitigate the beam split effect and enhance the security performance (Hu XY et al., 2024; Zhang YC et al., 2024).

6 Engineering and standardization

Sections 2–5 reviewed notable achievements in near-field technology from academic research. In the realms of engineering and standardization, near-field technology has also made significant breakthroughs. This section explores several key areas, including the primary spectrum for 6G networks, technologies for constructing near-field propagation, network deployment strategies, and standardization efforts.

6.1 6G spectrum

As mentioned in Section 2, the near-field distance increases with increasing frequency for a given antenna aperture size. In comparison to traditional mobile communication systems, 6G networks will operate in higher-frequency bands, enabling 6G networks to achieve greater near-field coverage distances.

Currently, frequency bands below 6 GHz are fully occupied or will soon be occupied by existing 4G/5G

commercial networks. The future deployment of 6G networks will need to coexist with these 4G/5G networks for the foreseeable future, making it difficult to free up the occupied sub-6 GHz frequency bands for 6G use in the short term. However, several newly allocated frequency bands above 6 GHz are expected to serve as primary bands for 6G networks, such as the U6G (6 GHz upper band, i.e., 6425–7125 MHz) (3GPP officially defines U6G (6425–7125 MHz) licensed spectrum, http://cdnuiy.uiycom.com/News/3GPP_Officially_Defines_U6G_6425-7125_MHz_Licensed_Spectrum/), upper mid-bands (7–24 GHz), mmWave, and even sub-THz bands. These bands offer wide bandwidth and favorable propagation characteristics, making them well-suited to meet the demands of future cellular networks.

In May 2023, China's Ministry of Industry and Information Technology (MIIT) issued a new version of the Regulations of the People's Republic of China on the Division of Radio Frequencies (MIIT Decree No. 62), making China the first country to allocate all or part of the 6425–7125 MHz frequency band, totaling 700 MHz, for 5G-A/6G systems (Regulations on the Allocation of Radio Frequencies in the People's Republic of China, Order No. 62 of the Ministry of Industry and Information Technology of the People's Republic of China, https://www.gov.cn/govweb/gongbao/2023/issue_10646/202308/content_6898890.html). In December of the same year, the ITU held the World Radio Communication Conference 2023 (WRC-23) in Dubai, UAE, where a new round of revisions to the Radio Regulations was completed. This revision allocated 700 MHz of mid-band spectrum in the 6425–7125 MHz range for 6G use in most countries worldwide (ITU, 2023). In December 2023, 3GPP held a meeting in Edinburgh, UK, where a research project on channel modeling for the new 7–24 GHz spectrum was initiated (3GPP, 2023). According to a study on 6G mid-bands, new spectrum ranges of 4.400–4.800, 7.125–8.400, and 14.800–15.350 GHz are potentially available for 6G networks, subject to further review during the WRC-27 cycle (Next G Alliance, 2022).

6.2 Enabling technologies

Traditional research on near-field technology focuses primarily on BSs equipped with larger-scale, centrally deployed active-phased array antenna (APAA), typically operating at high frequencies. This setup generates significant near-field propagation effects around the BS, making it a suitable model for studying near-field propagation in individual BS configurations. However, for large-scale practical deployment, a pervasive near-field propagation environment is needed to leverage near-field characteristics anytime and anywhere, enabling higher communication rates and more precise sensing as well as localization capabilities. The centralized deployment of traditional ultra-large-scale APAAs presents significant challenges in this context. Potential key technologies for 6G networks, such as novel APAAs, cell-free architectures (i.e., cell-free massive MIMO), and RIS, offer promising solutions to overcome these challenges and create a ubiquitous near-field propagation environment.

6.2.1 Challenges in constructing ubiquitous near-field propagation environments

There are two major limitations to the construction of ubiquitous near-field propagation environments.

1. Rayleigh distance vs. effective Rayleigh distance

As the operating frequencies for future 6G networks increase and the size of antenna arrays grows, the near-field coverage distance, based on the typical Rayleigh distance criterion, will significantly expand. However, the actual effective near-field distance is typically shorter than the Rayleigh distance (Wu ZD et al., 2023). This discrepancy indicates that the theoretical near-field coverage may not fully represent real-world conditions, necessitating the consideration of additional practical factors during deployment.

2. Near-field distance in off-axis regions

The Rayleigh distance criterion applies primarily to near-axial regions, achieving the maximum distance along the normal line. However, in off-axis regions, the near-field distance decreases as the deviation from the axis increases (Wu ZD et al., 2023). This means that near-field distance of the antenna array may be significantly reduced in practical applications due to the increase in off-axis angles.

In addition to these technical challenges, engineering practice must inevitably address typical concerns such as cost, power consumption, and deployment complexity.

6.2.2 New types of APAA

As frequency escalates, traditional APAAs require more antenna elements to maintain a comparable aperture size. Moreover, due to the complexities of the manufacturing process, the cost per element tends to increase considerably at higher frequencies, leading to a substantial rise in the overall cost of APAAs.

To implement large-sized array antennas cost-effectively at high frequencies, several novel active phased array schemes have been proposed in the literature (Li XR et al., 2022, 2023a; Wang HZ and Zeng, 2023; Zhu et al., 2023; Zhao YJ et al., 2024). These approaches can be broadly categorized into two technical approaches. The first approach is the RIS-based phased array antennas. Zhao YJ et al. (2024) (in Section 6.3) suggested using RIS as analog antenna arrays for the transmitter, replacing all or part of the analog arrays in hybrid beamforming architectures while retaining baseband signal processing outside the RIS. This approach can significantly reduce the cost and power consumption of BSs by replacing traditional phased array antennas with RIS. The second approach employs a sparse array structure for the phased arrays, aiming to reduce costs by decreasing the number of antenna elements. Li XR et al. (2022, 2023a) proposed a novel modular APAA architecture. Each module consists of a moderate/flexible number of array antennas with inter-element spacing typically on the order of the signal wavelength. Different modules were separated by relatively large inter-module distances, allowing practical conformal deployment. In Wang HZ and Zeng (2023), a uniformly sparse array structure with unit spacing greater than half the wavelength was proposed. However, similar to modular ELAA, the uniform sparse ELAA introduces undesired grating lobes due to the large inter-element spacing. Recently, the movable antenna (MA) technology has been introduced in wireless communication systems to control the local movement (position and/or rotation) of antennas at the transmitter/receiver, thereby improving wireless channel conditions and communication performance (Zhu et al., 2023). Unlike ELAA, which requires a large number of antenna elements and RF front-ends, the number of MAs remains moderate and can be kept constant, even as the moving region size increases. MAs offer the advantage of reducing the hardware costs and RF power consumption compared to ELAA.

6.2.3 Cell-free massive MIMO

Continuing with the traditional centralized antenna array deployment model would require several times deployment density compared to conventional far-field networks to ensure continuous near-field propagation coverage. This would result in higher costs due to the increased number of BSs and present challenges in finding suitable sites for high-density BS deployment.

A significant trend in the future development of multi-antenna technologies is the shift from centralized systems to distributed ones. Cell-free technology, formerly known as coordinated multipoint (CoMP), represents a leading distributed multi-antenna approach. By deploying numerous antennas cooperatively across an entire coverage area, cell-free systems can effectively create a pervasive and robust near-field propagation environment. This distributed deployment enables more efficient signal transmission and coverage, thereby addressing many issues associated with centralized antenna deployment in near-field scenarios.

Cell-free massive MIMO is considered a critical potential technology for 6G networks. Cell-free is a general term. When each distributed node is equipped with a massive antenna array, it is referred to as a cell-free massive MIMO. It involves distributed deployment, with each node typically equipped with a large-scale antenna array. Given the shorter distance between these nodes and the UE, the UE is highly likely to be within the near-field propagation region, especially when operating in mid-to-high-frequency bands. Consequently, research on 6G cell-free massive MIMO should consider the near-field propagation model as a fundamental assumption. In other words, cell-free massive MIMO is essential for enabling ubiquitous near-field propagation in future networks. However, compared to traditional far-field propagation models, cell-free massive MIMO based on the near-field propagation will encounter additional challenges.

Since the 4G LTE era, CoMP technology has been a topic of discussion and integration into the standards. Solutions introduced in the 4G standard, including features such as the zero-power CSI reference signal (CSI-RS) and UE-specific CSI-RS, addressed the basic functionalities required to support CoMP (Huawei, 2009a, 2009b; ZTE, 2011). However, widespread commercialization has not yet been

realized. Although CoMP technology is included in the 5G standard, with coherent CoMP joint transmission (CoMP-JT) being standardized, current implementations involve only non-coherent CoMP-JT. The predominant benefits of CoMP come from coherent CoMP-JT, while the gains from non-coherent CoMP-JT are limited, hindering widespread commercial adoption. The primary hurdle in implementing coherent CoMP with traditional active phased arrays lies in the intricate problem of mutual calibration of the antennas.

In massive, geographically distributed access points (APs) and users within cell-free MIMO (CF MIMO) systems, signals from different APs typically experience varying propagation delays, making time synchronization among received signals essential for coherent transmission. It is crucial to maintain time synchronization and phase alignment between different APs (Xu HQ et al., 2012; Rogalin et al., 2014). The synchronization accuracy requirements in CF MIMO networks become more stringent as user time sensitivity increases, particularly in near-field propagation scenarios. Various time synchronization schemes have been proposed to tackle this challenge, including one-way message dissemination, two-way message exchange, and receiver-only synchronization. These schemes typically manage timing misalignment by estimating clock offset and skew (Li BQ et al., 2022). Additionally, for accurate CSI at APs, phase calibration of uplink transmitted signals is essential, often achieved using a reference signal for over-the-air reciprocity calibration (Cao et al., 2023).

Furthermore, while communication services typically benefit from NLoS multipath environments, the ideal propagation environment for sensing, positioning, and wireless power transmission services is the near-field LoS channel. Centralized APAAs may place the target in a NLoS multipath channel. In contrast, distributed deployment facilitates the establishment of virtual LoS links with users or perceived objects, thereby increasing the probability of achieving LoS links compared to centralized deployment.

6.2.4 Reconfigurable intelligent surfaces

While distributed antenna technologies address some challenges of centralized APAA deployments, they remain limited by the technical constraints of APAAs, making dense and ubiquitous deployment difficult. Ultra-large APAAs increase hardware costs, complexity, power consumption, weight, and volume, which complicates dense deployments and limits near-field coverage. RIS offers unique technical advantages that effectively address these challenges. Using RIS-based distributed antenna arrays, near-field regions can be more flexibly covered, reducing reliance on individual sites, lowering deployment costs, and increasing site selection flexibility.

RISs, which use passive regulation and lack the need for channel reciprocity calibration, offer a viable solution for achieving coherent CoMP-JT. A practical approach to realizing coherent CoMP involves substituting RIS for traditional active phased arrays (Zhao, 2024d). However, RIS-based coherent CoMP-JT faces additional challenges, particularly in addressing synchronization during collaborative regulation among multiple RISs. Zhao YJ (2024b) explored potential solutions, proposing a network control mode, in which the BS coordinates multiple RISs to adjust phase alignment, thereby avoiding phase differences among them.

The unique technological advantages of RIS facilitate the creation of ubiquitous near-field propagation environments (Zhao, 2024b). First, as programmable two-dimensional EM metasurfaces, RISs can passively control EM waves, offering the advantages of low cost and low power consumption. This allows the creation of large antenna apertures at low cost, thereby facilitating dense deployments. Second, RISs can flexibly adapt to complex and diverse deployment environments due to their various types. From a functional perspective, RISs include channel regulation types (e.g., reflective RIS, transmissive RIS, and simultaneous transmitting and reflecting RIS (STAR-RIS) (Liu YW et al., 2023b)), information modulation types (e.g., RIS-based new transmitter, RIS-based backscatter transmitters, and RIS-based companion communications), and RIS-based new phased array antennas (Zhao, 2023). RIS can be manufactured into different sizes, shapes, and surface forms to meet various deployment needs. Finally, the simple and easy-to-deploy nature of RISs supports the creation of near-field LoS environments, better serving the requirements for sensing, positioning, and wireless power transmission. Additionally, because RISs are passive, they inherently have low EM radiation levels, ensuring compliance with specific absorption rate standards for human EM radiation safety in ubiquitous near-field environments.

Furthermore, RIS-based systems can more easily implement non-planar or conformal antenna arrays, which can help overcome the rapid near-field distance decline experienced by traditional planar antenna arrays when deviating from the near axis.

Existing RISs typically exhibit broadband characteristics, which, while tuning signals in the target spectrum, affect non-target signals and lead to significant network coexistence challenges (Zhao and Jian, 2021; Zhao and Lv, 2022). Various solutions were proposed to effectively mitigate this issue (Zhao and Jian, 2021; Zhao and Lv, 2022; Gürgünoğlu et al., 2024; Liang et al., 2024).

In summary, compared to traditional APAAs, RISs offer passive regulation, low cost, and easy deployment, enabling dense and widespread deployment. This makes RISs a promising technology for creating a ubiquitous near-field channel environment for future 6G networks.

6.3 Network deployment

The introduction of a ubiquitous near-field propagation environment will bring about a new network paradigm in the upcoming 6G networks. However, this paradigm shift presents a significant array of challenges that require thorough consideration and innovative solutions.

6.3.1 Challenges of integrated communication–sensing–energizing networks

Future 6G networks will integrate communication, sensing, and energy transfer capabilities, vastly expanding the functions of wireless networks. However, these three types of services differ substantially, posing considerable challenges to network deployment.

First, the distribution of these services varies. Communication services target a wide range of communication terminals connected to the network, while sensing services focus not only on communication terminals, but also on non-communication targets. On the contrary, energizing services primarily cater to low-power IoT devices. The geographical distribution and service characteristics of these three services differ significantly.

Second, the ideal propagation channel differs for each service; NLoS channels are preferable for communication services, whereas LoS channels are more suitable for sensing and energy transfer services. In addition, designing integrated waveforms for communication, sensing, and energy transfer poses a challenge due to the distinct waveform requirements for data transmission, sensing, positioning, and wireless energy transfer. Meeting the diverse needs of these three types of services, while achieving low-cost and low-complexity RIS-based near-field network deployment, presents substantial challenges for future 6G networks.

6.3.2 Changes in deployment optimization objectives

In traditional cellular network deployment based on far-field assumptions, the primary optimization objective is the signal strength distribution across the network, known as the link budget. However, in near-field-assumption-based network deployment, the optimization objective must consider not only signal strength distribution but also the changes in spatial freedom caused by near-field propagation characteristics (Zhao, 2024c). Therefore, optimizing near-field network deployment requires consideration of factors such as near-field distance conditions, RIS size, deployment density, and angles relative to the coverage area.

6.4 Standardization efforts

Standardization is crucial for enabling large-scale commercialization of communication technologies.

6.4.1 Standardization research and protocol design

The standardization and protocol design for near-field communications encompasses two primary areas: near-field channel modeling and near-field communication protocol design.

1. Near-field channel modeling

The existing 5G channel model standard, TR38.901 (ETSI, 2020), is based on the far-field assumption, which introduces biases when evaluating near-field technologies. In December 2023, the 3GPP approved a project to enhance the 7–24 GHz channel model during the RAN#102 Plenary Meeting (3GPP, 2023). This project aims to extend the TR38.901 channel model standard by incorporating new frequency bands, near-field propagation, and spatial non-stationary characteristics. These enhancements address the limitations of the current 5G channel model and fulfill the evaluation needs for future near-field applications. The project objective is to support research and evaluation

related to 6G standardization, reflecting a preliminary industry consensus on the potential significance of near-field technology for 6G developments.

2. Near-field communication protocol design

Standardization of near-field communication protocols involves two key components: developing general standardized protocols that establish near-field technology as a common foundational feature and optimizing protocol designs in conjunction with other 6G technologies such as RIS, ELAA, ISAC, and wireless power transfer (WPT).

(1) General standard protocol design for near-field technology

The design of standardized protocols for near-field technology encompasses various aspects such as channel estimation, beamforming, codebook design, and beam training. Current 5G standards assume that users operate in the far field, treating EM waves as plane waves. However, directly applying these solutions to near-field scenarios would degrade system performance, highlighting the need for technical solutions specifically suited to spherical wave channels. In terms of beamforming, unlike far-field communication where beamforming is restricted to the angular domain, near-field communication based on spherical wave assumptions allows for beam focusing. Using polar coordinates, beams can be optimized not only in the angular domain but also in the distance domain for near-field applications. Therefore, customized beam training and codebook design are necessary for the near-field environment.

(2) Optimized standard protocol design with 6G key technologies

Many potential key technologies of the 6G wireless air interface, such as RIS, ELAA, ISAC, and WPT, must account for the near-field effect when optimizing standard protocol design during the standardization process. This involves establishing channel models for these technologies in the near-field region and developing technical solutions to optimize beamforming, channel estimation, and codebook design specifically for the near-field environment.

6.4.2 Standardization activities

Recently, several organizations have undertaken activities to promote the standardization of near-field technology, advancing research in this area significantly.

1. In December 2023, 3GPP 5G Release 19 approved the 7–24 GHz Channel Measurement and Modeling Research Project, with a key focus on near-field characteristics (work item rapporteurs: Daewon LEE with Intel and Nan ZHANG with ZTE Corporation) (3GPP, 2023).

2. On March 15, 2024, ZTE Corporation led the successful establishment of the "Near-Field Model and Mechanism Project" in ETSI ISG RIS (Zheng S, 2024).

3. On April 18, 2024, the New Technologies and Materials Sub-Forum of the 6G Conference released the 6G Near-Field Technology White Paper (https://www.c114.com.cn/wireless/2935/a1261616.html).

4. On April 25, 2024, ZTE Corporation, in collaboration with China's three major telecom operators, initiated a near-field technology research project under the CCSA TC5WG6 (https://www.ccsa.org.cn/).

5. On April 27, 2024, the initiative 6G Near-Field Technologies Research and Standardization was released at the first Near-Field Communication Theory and Application Forum hosted by the Institute of Electronics (https://mp.weixin.qq.com/s/0Hpjf-ETKwvGPH_K-SyQIQ).

7 Future trends and challenges

This section explores several future research directions related to the near-field technology which are expected to have a significant impact on system design.

7.1 Distributed transmission from a near-field perspective

Current research on near-field signal processing focuses predominantly on centralized arrays. However, in distributed MIMO systems, APs that spread across different regions can be treated as part of a large and sparse array, making it feasible to apply the near-field theory to distributed transmissions. For instance, the concept of network ELAA introduced in Wang JF et al. (2022) envisions multiple APs arranged at equal intervals along a line, each equipped with a ULA. Similarly, Li XR et al. (2023b) explored a model known as modular MIMO. These studies feature antennas distributed in a significant regular pattern. Future research could explore the application of near-field theory to

channel models with randomly positioned antennas, which may reduce feedback overhead and enhance beamforming gains, offering promising advancements in the efficiency and performance of distributed MIMO systems in near-field scenarios.

7.2 Tri-polarized transmission in the near field

The existing far-field transmission scheme is limited to two polarization directions, which are used for spatial multiplexing. In the context of ELAA in the near field, an additional polarization axis can be exploited to use the EM spectrum more efficiently, resulting in higher data rates and improved spectral efficiency (Wei et al., 2023).

Despite these advantages, near-field tri-polarized transmission faces several challenges. First, accurate channel models that capture the transmission characteristics in all polarization directions are essential, often requiring complex EM simulations. These models must account for the interactions of EM waves in a tri-polarized environment, adding complexity to system design and analysis. Moreover, the electric field amplitude along the extra polarization direction attenuates rapidly, imposing strict requirements on the spatial distribution of users. Maintaining adequate signal strength across all polarization directions becomes challenging over longer distances. Consequently, practical application of near-field tri-polarization transmission requires careful consideration of user placement and system design to achieve the optimal performance.

7.3 Mobility in the near field

Compared to far-field propagation environments, near-field propagation conditions present more significant mobility challenges (Zhao, 2024c): (1) Beam's focal spot is smaller, resulting in greater variations in signal strength when the UE moves even slightly. This leads to fluctuations in data transmission rates, sensing performance, and energy transfer efficiency. (2) The spatial DoFs vary significantly depending on the distance and angle relative to the antenna aperture, impacting spatial multiplexing gains and the capacity of space-division multiple access. (3) Mobility may cause beam misalignment, necessitating the re-establishment of positioning, which introduces delays. Additionally, sensing tasks may lose track of targets due to mobility.

To address mobility challenges in near-field propagation, the following strategies can be considered:

1. Specialized beam design: optimizing non-diffractive beams or developing broadband beams specifically tailored for near-field propagation environments can better accommodate the demands of mobile scenarios.

2. Dynamic beam tracking: in ISAC scenarios, leveraging real-time location information can assist in dynamic beam tracking.

3. CSI measurement and feedback: designing more efficient and timely CSI measurement and feedback mechanisms will enable precise dynamic tracking for beam control.

4. Robust codebooks: develop robust codebooks that can adapt to dynamic changes.

5. Signaling procedures: establish signaling protocols for seamless cell or regional switching in near-field environments.

6. ELAA/RIS deployment: optimize ELAA/RIS deployment to minimize changes in near-field propagation characteristics.

7.4 Sensing in the near field

Current research on wireless sensing focuses mainly on far-field source sensing, where the phase rotations resulting from targets' multi-dimensional parameters are decoupled across different domains (Hu ZL et al., 2024; Zhang J et al., 2024). In contrast, near-field source sensing involves phase rotations that are mutually coupled across these domains. Thus, compared to far-field sensing, near-field sensing has significant advantages (Liu YW et al., 2023a). On one hand, the coupling of multi-dimensional parameters enhances sensing accuracy due to the higher degree of freedom. This coupling allows the sensing performance of a particular-dimension parameter to be improved by using the signal observations from multiple dimensions. On the other hand, due to the spherical wave characteristics in the near field, more parameters can be sensed. For example, the near-field targets' tangential velocities can be estimated across spatial and temporal domains.

However, near-field sensing faces great challenges:

1. Design of low-complexity sensing algorithms. The ultra-large-scale MIMO antennas introduce extremely high, and sometimes unmanageable computational

complexity for on-grid sensing algorithms. This coupling of multi-dimensional parameters renders mainstream off-gird low-complexity sensing algorithms, such as discrete-Fourier-transform (DFT) and ESPRIT algorithms, invalid for near-field sensing.

2. Design of the sensing algorithm with multi-carrier waveforms. Most literature on near-field sensing (Zheng Z et al., 2018; Molaei AM et al., 2020, 2022) focuses on single-carrier sensing waveforms. However, these approaches are not applicable to near-field systems using multiple carrier waveforms like orthogonal frequency division multiplex (OFDM), where the phase rotations across space and frequency domains are multiplicatively coupled.

7.5 WPT in the near field

WPT technology offers a promising solution for wirelessly charging electronic devices (Mohsan et al., 2023), with vast potential in the era of 6G networks and IoT. Current WPT technology faces challenges in far-field scenarios due to low energy transfer efficiency. However, in the near-field scenarios of 6G networks, various energy transmission beams can focus the energy of the RF signals to the vicinity of the energy receivers, significantly enhancing the energy transfer efficiency. Moreover, by controlling the energy distribution of these beams, it is possible to reduce EM pollution in non-target areas, further enhancing the environmental impact of WPT. This advancement increases the potential of WPT technology, making it a crucial component in the development of efficient and environmentally friendly wireless charging solutions.

8 Conclusions

This paper presents a thorough overview of state-of-the-art advancements in near-field technology research, emphasizing its critical role in enhancing 6G communication systems. We began by exploring the fundamental characteristics of near-field propagation, including its definitions, transmission properties, and performance metrics. Subsequently, we delved into near-field channel models and measurement results, covering deterministic, stochastic, and EM information theory based models. As channel models evolve, we underscored the importance of redesigning and optimizing traditional mechanisms, particularly in areas such as channel estimation, beam training, and codebook design, to align with the distinctive characteristics of near-field propagation. We also introduced innovative beam designs facilitated by near-field technologies, including non-diffractive beams (such as Bessel and Airy) and OAM beams, which have the potential to revolutionize near-field communication systems. Furthermore, we discussed significant progress in engineering and standardization efforts related to these technologies, addressing key areas such as the primary 6G spectrum and enabling technologies for near-field propagation. Finally, we outlined several promising research directions that could have a profound impact on system design in this rapidly evolving field.

In conclusion, this comprehensive review offers a detailed overview of the current state and potential of near-field technologies, underscoring their crucial role in advancing communication systems for 6G networks and beyond. We hope that this work will serve as a valuable resource for researchers and practitioners in the field of near-field communications.

Contributors

Yajun ZHAO initialized the project. All the authors drafted and revised the paper.

Conflict of interest

Yajun ZHAO and Linglong DAI are executive lead editors of this special issue. Jianhua ZHANG, Zhi CHEN, Yuanwei LIU, Chongwen HUANG, and Long LI are guest editors of this special issue. Ping ZHANG is the editor-in-chief of this special issue. Also, Jianhua ZHANG, Chau YUEN, and Ping ZHANG are executive associate editor-in-chief, editorial board member, and associate editor-in-chief of *Frontiers of Information Technology & Electronic Engineering*, respectively. They were not involved with the peer review process of this paper. All the authors declare that they have no conflict of interest.

References

3GPP, 2023. RP-234018, Channel Modelling Enhancements for 7-24 GHz. https://www.3gpp.org/ftp/tsg_ran/TSG_RAN/TSGR_102/Docs/RP-234018.zip

Abdou A, 2023. Super-Airy beams. *Opt Expr*, 31(24):39447-39453. https://doi.org/10.1364/OE.504205

Basar E, 2018. Orbital angular momentum with index modulation. *IEEE Trans Wirel Commun*, 17(3):2029-2037. https://doi.org/10.1109/TWC.2017.2787992

Björnson E, Demir ÖT, Sanguinetti L, 2021. A primer on near-field beamforming for arrays and reconfigurable intelligent surfaces. Proc 55th Asilomar Conf on Signals, Systems, and Computers, p.105-112. https://doi.org/10.1109/IEEECONF53345.2021.9723331

Bohagen F, Orten P, Oien GE, 2009. On spherical vs. plane wave modeling of line-of-sight MIMO channels. *IEEE Trans Commun*, 57(3):841-849. https://doi.org/10.1109/TCOMM.2009.03.070062

Cai XS, Fan W, Yin XF, et al., 2020. Trajectory-aided maximum-likelihood algorithm for channel parameter estimation in ultrawideband large-scale arrays. *IEEE Trans Antenn Propag*, 68(10):7131-7143. https://doi.org/10.1109/TAP.2020.2996774

Cao Y, Wang P, Zheng K, et al., 2023. Experimental performance evaluation of cell-free massive MIMO systems using COTS RRU with OTA reciprocity calibration and phase synchronization. *IEEE J Sel Areas Commun*, 41(6):1620-1634. https://doi.org/10.1109/JSAC.2023.3276057

Chen H, Elzanaty A, Ghazalian R, et al., 2022. Channel model mismatch analysis for XL-MIMO systems from a localization perspective. IEEE Global Communications Conf, p.1588-1593. https://doi.org/10.1109/GLOBECOM48099.2022.10000613

Chen KJ, Qi CH, Wang CX, et al., 2024. Beam training and tracking for extremely large-scale MIMO communications. *IEEE Trans Wirel Commun*, 23(5):5048-5062. https://doi.org/10.1109/TWC.2023.3324176

Chen R, Long WX, Wang XD, et al., 2020. Multi-mode OAM radio waves: generation, angle of arrival estimation and reception with UCAs. *IEEE Trans Wirel Commun*, 19(10):6932-6947. https://doi.org/10.1109/TWC.2020.3007026

Chen YB, Wang Y, Wang ZC, et al., 2024. Angular-distance based channel estimation for holographic MIMO. *IEEE J Sel Areas Commun*, 42(6):1684-1702. https://doi.org/10.1109/JSAC.2024.3389116

Cheng Q, Jin S, Cui TJ, 2023. Reconfigurable intelligent surfaces for wireless communications. *Front Inform Technol Electron Eng*, 24(12):1665-1668. https://doi.org/10.1631/FITEE.2320000

Cui MY, Dai LL, 2022. Channel estimation for extremely large-scale MIMO: far-field or near-field? *IEEE Trans Commun*, 70(4):2663-2677. https://doi.org/10.1109/TCOMM.2022.3146400

Cui MY, Dai LL, 2024. Near-field wideband beamforming for extremely large antenna arrays. *IEEE Trans Wirel Commun*, 23(10):13110-13124. https://doi.org/10.1109/TWC.2024.3398770

Cui MY, Wu ZD, Lu Y, et al., 2023a. Near-field MIMO communications for 6G: fundamentals, challenges, potentials, and future directions. *IEEE Commun Mag*, 61(1):40-46. https://doi.org/10.1109/MCOM.004.2200136

Cui MY, Dai LL, Wang ZC, et al., 2023b. Near-field rainbow: wideband beam training for XL-MIMO. *IEEE Trans Wirel Commun*, 22(6):3899-3912. https://doi.org/10.1109/TWC.2022.3222198

Cui TJ, Jin S, Zhang JY, et al., 2021. Research Report on Reconfigurable Intelligent Surface Technology (in Chinese). IMT-2030 (6G) Promotion Group, Beijing, China. https://www.imt2030.org.cn/html//default/zhongwen/chengguofabu/yanjiubaogao/list-7.html?index=2

Cui Z, Liu J, Yang G, 2024. XL-RIS empowered near-field physical layer security against jamming and eavesdropping attacks. *Front Inform Technol Electron Eng*, 25(12):1750-1758. https://doi.org/10.1631/FITEE.2400477

Demir ÖT, Björnson E, Sanguinetti L, 2022. Channel modeling and channel estimation for holographic massive MIMO with planar arrays. *IEEE Wirel Commun Lett*, 11(5):997-1001. https://doi.org/10.1109/LWC.2022.3152600

Dong ZJ, Zeng Y, 2022. Near-field spatial correlation for extremely large-scale array communications. *IEEE Commun Lett*, 26(7):1534-1538. https://doi.org/10.1109/LCOMM.2022.3170735

ETSI, 2020. ETSI TR 138 901 V16.1.0 (2020-11), Study on Channel Model for Frequencies from 0.5 to 100 GHz. V16.1.0. Technical Report 38.901 (3GPP TR 38.901 version 16.1.0 Release16). https://www.etsi.org/deliver/etsi_tr/138900_138999/138901/16.01.00_60/tr_138901v160100p.pdf

Ettorre M, Pavone SC, Casaletti M, et al., 2018. Near-field focusing by non-diffracting Bessel beams. In: Boriskin A, Sauleau R (Eds.), Aperture Antennas for Millimeter and Sub-Millimeter Wave Applications. Springer, Cham, p.243-288. https://doi.org/10.1007/978-3-319-62773-1_8

Fan JB, Chen R, Long WX, et al., 2021. Radio-frequency multi-mode OAM detection based on UCA samples learning. Proc IEEE 22nd Int Workshop on Signal Processing Advances in Wireless Communications, p.56-60. https://doi.org/10.1109/SPAWC51858.2021.9593109

Feng C, Lu HQ, Zeng Y, et al., 2023. Near-field modeling and performance analysis for extremely large-scale IRS communications. *IEEE Trans Wirel Commun*, 23(5):4976-4989. https://doi.org/10.1109/TWC.2023.3323770

Feng Q, Kong XD, Shan MM, et al., 2022. Multi-orbital-angular-momentum-mode vortex wave multiplexing and demultiplexing with shared-aperture reflective metasurfaces. *Phys Rev Appl*, 17(3):0340171.

https://doi.org/10.1103/PhysRevApplied.17.034017

Franceschetti M, Migliore MD, Minero P, et al., 2015. The information carried by scattered waves: near-field and non-asymptotic regimes. *IEEE Trans Antenn Propag*, 63(7): 3144-3157. https://doi.org/10.1109/TAP.2015.2429742

Fuschini F, Zoli M, Vitucci EM, et al., 2019. A study on millimeter-wave multiuser directional beamforming based on measurements and ray tracing simulations. *IEEE Trans Antenn Propag*, 67(4):2633-2644. https://doi.org/10.1109/TAP.2019.2894271

Gao HQ, Kyösti P, Zhang X, et al., 2023. Digital twin enabled 6G radio testing: concepts, challenges and solutions. *IEEE Commun Mag*, 61(12):88-94. https://doi.org/10.1109/MCOM.001.2200860E

Gao S, Dong PH, Pan ZW, et al., 2024. Lightweight deep learning based channel estimation for extremely large-scale massive MIMO systems. *IEEE Trans Veh Technol*, 73(7): 10750-10754. https://doi.org/10.1109/TVT.2024.3364510

Gao TY, Tang P, Tian L, et al., 2023. A 3GPP-like channel simulation framework considering near-field spatial non-stationary characteristics of massive MIMO. IEEE Globecom Workshops, p.1493-1498. https://doi.org/10.1109/GCWkshps58843.2023.10464808

Gong TR, Wei L, Yang ZJ, et al., 2023a. A generalized electromagnetic-domain channel modeling for LOS holographic MIMO with arbitrary surface placements. IEEE Int Conf on Communications Workshops, p.1222-1227. https://doi.org/10.1109/ICCWorkshops57953.2023.10283739

Gong TR, Wei L, Huang CW, et al., 2023b. Holographic MIMO communications with arbitrary surface placements: near-field LoS channel model and capacity limit. *IEEE J Sel Areas Commun*, 42(6):1549-1566. https://doi.org/10.1109/JSAC.2024.3389126

Gong TR, Gavriilidis P, Ji R, et al., 2023c. Holographic MIMO communications: theoretical foundations, enabling technologies, and future directions. *IEEE Commun Surv Tut*, 26(1):196-257. https://doi.org/10.1109/COMST.2023.3309529

Gong TR, Huang CW, He JG, et al., 2023d. A transmit-receive parameter separable electromagnetic channel model for LoS holographic MIMO. Proc IEEE Global Communications Conf, p.5701-5706. https://doi.org/10.1109/GLOBECOM54140.2023.10437544

Gürgünoğlu D, Björnson E, Fodor G, 2024. Combating inter-operator pilot contamination in reconfigurable intelligent surfaces assisted multi-operator networks. *IEEE Trans Commun*, 72(9):5884-5895. https://doi.org/10.1109/TCOMM.2024.3390095

Han C, Bicen AO, Akyildiz IF, 2015. Multi-ray channel modeling and wideband characterization for wireless communications in the terahertz band. *IEEE Trans Wirel Commun*, 14(5):2402-2412. https://doi.org/10.1109/TWC.2014.2386335

Han C, Chen YH, Yan LF, et al., 2024. Cross far- and near-field wireless communications in terahertz ultra-large antenna array systems. *IEEE Wirel Commun*, 31(3):148-154. https://doi.org/10.1109/MWC.003.2300004

Han JQ, Li L, Yi H, et al., 2018. Versatile orbital angular momentum vortex beam generator based on reconfigurable reflective metasurface. *Jpn J Appl Phys*, 57(12):120303. https://doi.org/10.7567/JJAP.57.120303

Han Y, Jin S, Wen CK, et al., 2020. Channel estimation for extremely large-scale massive MIMO systems. *IEEE Wirel Commun Lett*, 9(5):633-637. https://doi.org/10.1109/LWC.2019.2963877

Haneda K, Takada JI, Kobayashi T, 2006. A parametric UWB propagation channel estimation and its performance validation in an anechoic chamber. *IEEE Trans Microw Theory Technol*, 54(4):1802-1811. https://doi.org/10.1109/TMTT.2006.871990

Hu S, Ilter MC, Wang H, 2022. Near-field beamforming for large intelligent surfaces. IEEE 33rd Annual Int Symp on Personal, Indoor and Mobile Radio Communications, p.1367-1373. https://doi.org/10.1109/PIMRC54779.2022.9977582

Hu XY, Zhang Y, Yang LX, et al., 2024. Securing near-field wideband MIMO communications via true-time delayer-based hybrid beamfocusing. *IEEE Trans Wirel Commun*, 23(10):13562-13578. https://doi.org/10.1109/TWC.2024.3403995

Hu ZL, Ye QB, Huang YX, et al., 2024. Joint range-velocity-azimuth estimation for OFDM-based integrated sensing and communication. *IEEE Trans Wirel Commun*, 23(10): 12933-12948. https://doi.org/10.1109/TWC.2024.3397312

Huawei, 2009a. R1-092364 Consideration on CSI-RS Design for CoMP and Text Proposal to 36.814. https://www.3gpp.org/ftp/tsg_ran/WG1_RL1/TSGR1_57b/Docs/R1-092364.zip

Huawei, 2009b. R1-093031 Consideration on CSI-RS Design for CoMP and Text Proposal to 36.814. https://www.3gpp.org/ftp/tsg_ran/WG1_RL1/TSGR1_58/Docs/R1-093031.zip

IMT-2030 (6G) Promotion Group, 2022. 6G Typical Scenarios and Key Capabilities White Paper (in Chinese). https://www.imt2030.org.cn/html/default/zhongwen/chengguofabu/baipishu/index.html?index=2

ITU, 2023. WRC-23 Booklet: Agenda and Relevant Resolutions. https://www.itu.int/wrc-23/booklet-wrc-23/

ITU-R WP5D, 2023. Framework and Overall Objectives of the Future Development of IMT for 2030 and Beyond. https://www.itu.int/rec/R-REC-M.2160/en

Ji R, Chen S, Huang CW, et al., 2023. Extra DoF of near-field holographic MIMO communications leveraging evanescent waves. *IEEE Wirel Commun Lett*, 12(4):580-584. https://doi.org/10.1109/LWC.2023.3234003

Jiang JS, Ingram MA, 2005. Spherical-wave model for short-range MIMO. *IEEE Trans Commun*, 53(9):1534-1541. https://doi.org/10.1109/TCOMM.2005.852842

Jiang YH, Gao FF, 2023. Electromagnetic channel model for near field MIMO systems in the half space. *IEEE Commun Lett*, 27(2):706-710. https://doi.org/10.1109/LCOMM.2022.3229445

Kadlimatti R, Parimi PV, 2019. Millimeter-wave nondiffracting circular Airy OAM beams. *IEEE Trans Antenn Propag*,

67(1):260-269. https://doi.org/10.1109/TAP.2018.2876713

Karstensen A, Fan W, Carton I, et al., 2016. Comparison of ray tracing simulations and channel measurements at mmWave bands for indoor scenarios. 10th European Conf on Antennas and Propagation, p.1-5. https://doi.org/10.1109/EuCAP.2016.7481361

Khonina SN, Kazanskiy NL, Karpeev SV, et al., 2020. Bessel beam: significance and applications—a progressive review. *Micromachines*, 11(11):997. https://doi.org/10.3390/mi11110997

Lee A, Ju H, Kim S, et al., 2022. Intelligent near-field channel estimation for terahertz ultra-massive MIMO systems. Global Communications Conf, p.5390-5395. https://doi.org/10.1109/GLOBECOM48099.2022.10001612

Lee D, Sasaki H, Yagi Y, et al., 2023. Orbital angular momentum multiplexing using radio wave and its extension to multishape radio. *J Lightw Technol*, 41(7):1985-1996. https://doi.org/10.1109/JLT.2022.3223366

Lei H, Zhang JY, Xiao HH, et al., 2024. Channel estimation for XL-MIMO systems with polar-domain multi-scale residual dense network. *IEEE Trans Veh Technol*, 73(1): 1479-1484. https://doi.org/10.1109/TVT.2023.3311010

Li BQ, Zhu X, Jiang YF, et al., 2022. Cooperative time synchronization and parameter estimation via broadcasting for cell-free massive MIMO networks. Proc IEEE Wireless Communications and Networking Conf, p.2100-2105. https://doi.org/10.1109/WCNC51071.2022.9771548

Li JZ, Ai B, He RS, et al., 2018. The 3D spatial non-stationarity and spherical wavefront in massive MIMO channel measurement. Proc 10th Int Conf on Wireless Communications and Signal Processing, p.1-6. https://doi.org/10.1109/WCSP.2018.8555869

Li L, Xue H, Feng Q, 2018. Research progresses in theory and applications of vortex electromagnetic waves. *J Microw*, 34(2):1-12 (in Chinese). https://doi.org/10.14183/j.cnki.1005-6122.201802001

Li L, Zhang R, Cui TJ, 2023. Information metasurfaces and reconfigurable intelligent surfaces. *J Inform Intell*, 1(3): 179-181.https://doi.org/10.1016/j.jiixd.2023.07.001

Li MT, Yuan ZQ, Lyu YJ, et al., 2023. Gigantic MIMO channel characterization: challenges and enabling solutions. *IEEE Commun Mag*, 61(10):140-146. https://doi.org/10.1109/MCOM.001.2200969

Li N, Fan JB, Long WX, et al., 2023. Misalignment-robust OAM multi-mode multiplexing with index modulation based on UCA samples learning. IEEE 34th Annual Int Symp on Personal, Indoor and Mobile Radio Communications, p.1-5. https://doi.org/10.1109/PIMRC56721.2023.10294073

Li RW, Sun S, Tao MX, 2023. Applicable regions of spherical and plane wave models for extremely large-scale array communications. https://arxiv.org/abs/2301.06036

Li XR, Lu HQ, Zeng Y, et al., 2022. Near-field modeling and performance analysis of modular extremely large-scale array communications. *IEEE Commun Lett*, 26(7):1529-1533. https://doi.org/10.1109/LCOMM.2022.3172437

Li XR, Lu HQ, Zeng Y, et al., 2023a. Modular extremely large-scale array communication: near-field modelling and performance analysis. *China Commun*, 20(4):132-152. https://doi.org/10.23919/JCC.fa.2022-0715.202304

Li XR, Dong ZJ, Zeng Y, et al., 2023b. Near-field beam focusing pattern and grating lobe characterization for modular XL-array. IEEE Global Communications Conf, p.4068-4073. https://doi.org/10.1109/GLOBECOM54140.2023.10436773

Li XR, Dong ZJ, Zeng Y, et al., 2024. Multi-user modular XL-MIMO communications: near-field beam focusing pattern and user grouping. *IEEE Trans Wirel Commun*, 23(10):13766-13781. https://doi.org/10.1109/TWC.2024.3404659

Li ZR, Gao Z, Li T, 2023. Sensing user's channel and location with terahertz extra-large reconfigurable intelligent surface under hybrid-field beam squint effect. *IEEE J Sel Top Signal Process*, 17(4):893-911. https://doi.org/10.1109/JSTSP.2023.3278942

Lian YD, Qi X, Wang YH, et al., 2022. OAM beam generation in space and its applications: a review. *Opt Lasers Eng*, 151:106923. https://doi.org/10.1016/j.optlaseng.2021.106923

Liang JC, Zhang L, Luo ZJ, et al., 2024. A filtering reconfigurable intelligent surface for interference-free wireless communications. *Nat Commun*, 15(1):3838. https://doi.org/10.1038/s41467-024-47865-6

Lin MT, Gao Y, Liu PG, et al., 2017. Theoretical analyses and design of circular array to generate orbital angular momentum. *IEEE Trans Antenn Propag*, 65(7):3510-3519. https://doi.org/10.1109/TAP.2017.2700160

Liu J, Yang G, Liu YW, et al., 2024. RIS empowered near-field covert communications. *IEEE Trans Wirel Commun*, 23(10): 15477-15492. https://doi.org/10.1109/TWC.2024.3430328

Liu LF, Oestges C, Poutanen J, et al., 2012. The COST 2100 MIMO channel model. *IEEE Wirel Commun*, 19(6):92-99. https://doi.org/10.1109/MWC.2012.6393523

Liu Q, Chen ZN, Liu YN, et al., 2018. Circular polarization and mode reconfigurable wideband orbital angular momentum patch array antenna. *IEEE Trans Antenn Propag*, 66(4): 1796-1804. https://doi.org/10.1109/TAP.2018.2803757

Liu W, Ren H, Pan CH, et al., 2023a. Deep learning based beam training for extremely large-scale massive MIMO in near-field domain. *IEEE Commun Lett*, 27(1):170-174. https://doi.org/10.1109/LCOMM.2022.3210042

Liu W, Pan CH, Ren H, et al., 2023b. Low-overhead beam training scheme for extremely large-scale RIS in near field. *IEEE Trans Commun*, 71(8):4924-4940. https://doi.org/10.1109/TCOMM.2023.3278728

Liu W, Pan CH, Ren H, et al., 2024a. Near-field multiuser beam-training for extremely large-scale MIMO systems. *IEEE Trans Commun*, early access. https://doi.org/10.1109/TCOMM.2024.3468208

Liu W, Pan CH, Ren H, et al., 2024b. NMBEnet: efficient near-field mmWave beam training for multiuser OFDM systems

using sub-6 GHz pilots. https://arxiv.org/abs/2404.15469

Liu YM, Zhang JH, Zhang YX, et al., 2024. A shared cluster-based stochastic channel model for integrated sensing and communication systems. *IEEE Trans Veh Technol*, 73(5): 6032-6044. https://doi.org/10.1109/TVT.2023.3337648

Liu YW, Wang ZL, Xu JQ, et al., 2023a. Near-field communications: a tutorial review. *IEEE Open J Commun Soc*, 4: 1999-2049. https://doi.org/10.1109/OJCOMS.2023.3305583

Liu YW, Xu JQ, Wang ZL, et al., 2023b. Simultaneously transmitting and reflecting (STAR) RISs for 6G: fundamentals, recent advances, and future directions. *Front Inform Technol Electron Eng*, 24(12):1689-1707. https://doi.org/10.1631/FITEE.2300490

Liu ZL, Zhang JY, Liu ZH, et al., 2024. Cell-free XL-MIMO meets multi-agent reinforcement learning: architectures, challenges, and future directions. *IEEE Wirel Commun*, 31(4):155-162. https://doi.org/10.1109/MWC.007.2300176

Long WX, Chen R, Moretti M, et al., 2021a. AoA estimation for OAM communication systems with mode-frequency multi-time ESPRIT method. *IEEE Trans Veh Technol*, 70(5):5094-5098. https://doi.org/10.1109/TVT.2021.3070358

Long WX, Chen R, Moretti M, et al., 2021b. Joint spatial division and coaxial multiplexing for downlink multi-user OAM wireless backhaul. *IEEE Trans Broadcast*, 67(4): 879-893. https://doi.org/10.1109/TBC.2021.3081869

Long WX, Chen R, Moretti M, 2023. Recursive ESPRIT algorithm for multi-user OAM low-overhead AoA estimation. *IEEE Trans Veh Technol*, 72(2):2672-2677. https://doi.org/10.1109/TVT.2022.3212109

Lu HQ, Zeng Y, 2021. How does performance scale with antenna number for extremely large-scale MIMO? Proc IEEE Int Conf on Communications, p.1-6. https://doi.org/10.1109/ICC42927.2021.9500972

Lu HQ, Zeng Y, 2022. Communicating with extremely large-scale array/surface: unified modeling and performance analysis. *IEEE Trans Wirel Commun*, 21(6):4039-4053. https://doi.org/10.1109/TWC.2021.3126384

Lu HQ, Zeng Y, You CS, et al., 2024. A tutorial on near-field XL-MIMO communications towards 6G. *IEEE Commun Surv Tut*, 26(4):2213-2257. https://doi.org/10.1109/COMST.2024.3387749

Lu Y, Dai LL, 2023. Near-field channel estimation in mixed LoS/NLoS environments for extremely large-scale MIMO systems. *IEEE Trans Commun*, 71(6):3694-3707. https://doi.org/10.1109/TCOMM.2023.3260242

Lyu YJ, Yuan ZQ, Zhang FC, et al., 2023. Virtual antenna array for W-band channel sounding: design, implementation, and experimental validation. *IEEE J Sel Top Signal Process*, 17(4):729-744. https://doi.org/10.1109/JSTSP.2023.3301135

McGloin D, Dholakia K, 2005. Bessel beams: diffraction in a new light. *Contemp Phys*, 46(1):15-28. https://doi.org/10.1080/0010751042000275259

Meng XS, Chen XM, Yang L, et al., 2020. Launcher of high-order Bessel vortex beam carrying orbital angular momentum by designing anisotropic holographic metasurface. *Appl Phys Lett*, 117(24):243503. https://doi.org/10.1063/5.0031139

Mohammadi SM, Daldorff LKS, Bergman JES, et al., 2010. Orbital angular momentum in radio—a system study. *IEEE Trans Antenn Propag*, 58(2):565-572. https://doi.org/10.1109/TAP.2009.2037701

Mohsan SAH, Qian H, Amjad H, 2023. A comprehensive review of optical wireless power transfer technology. *Front Inform Technol Electron Eng*, 24(6):767-800. https://doi.org/10.1631/FITEE.2100443

Molaei AM, Zakeri B, Andargoli SMH, 2020. Components separation algorithm for localization and classification of mixed near-field and far-field sources in multipath propagation. *IEEE Tran Signal Process*, 68:404-419. https://doi.org/10.1109/TSP.2019.2961226

Molaei AM, del Hougne P, Fusco V, et al., 2022. Efficient joint estimation of DOA, range and reflectivity in near-field by using mixed-order statistics and a symmetric MIMO array. *IEEE Trans Veh Technol*, 71(3):2824-2842. https://doi.org/10.1109/TVT.2021.3138251

Mukherjee P, Gupta B, 2008. Terahertz (THz) frequency sources and antennas—a brief review. *Int J Infrared Milli Waves*, 29(12):1091-1102. https://doi.org/10.1007/s10762-008-9423-0

Myers NJ, Heath RW, 2022. InFocus: a spatial coding technique to mitigate misfocus in near-field LoS beamforming. *IEEE Trans Wirel Commun*, 21(4):2193-2209. https://doi.org/10.1109/TWC.2021.3110011

Nepa P, Buffi A, 2017. Near-field-focused microwave antennas: near-field shaping and implementation. *IEEE Antenn Propag Mag*, 59(3):42-53. https://doi.org/10.1109/MAP.2017.2686118

Next G Alliance, 2022. Next G Alliance Report: 6G Technologies. https://www.nextgalliance.org/wp-content/uploads/dlm_uploads/2022/07/TWG-report-6G-technologies.pdf

Ng KH, Tameh EK, Doufexi A, et al., 2007. Efficient multi-element ray tracing with site-specific comparisons using measured MIMO channel data. *IEEE Trans Veh Technol*, 56(3):1019-1032. https://doi.org/10.1109/TVT.2007.895606

Ning BY, Chen Z, Chen WR, et al., 2020. Channel estimation and transmission for intelligent reflecting surface assisted THz communications. Proc IEEE Int Conf on Communications, p.1-7. https://doi.org/10.1109/ICC40277.2020.9149153

Ouyang CJ, Liu YW, Yang HW, 2022. Performance of downlink and uplink integrated sensing and communications (ISAC) systems. *IEEE Wirel Commun Lett*, 11(9):1850-1854. https://doi.org/10.1109/LWC.2022.3184409

Ouyang CJ, Liu YW, Zhang XQ, et al., 2023. Near-field communications: a degree-of-freedom perspective. https://arxiv.org/abs/2308.00362

Pan YJ, Pan CH, Jin S, et al., 2023. RIS-aided near-field localization and channel estimation for the terahertz system. *IEEE J Sel Top Signal Process*, 17(4):878-892.

https://doi.org/10.1109/JSTSP.2023.3285431

Payami S, Tufvesson F, 2012. Channel measurements and analysis for very large array systems at 2.6 GHz. Proc 6th European Conf on Antennas and Propagation, p.433-437. https://doi.org/10.1109/EuCAP.2012.6206345

Pizzo A, Marzetta T, Sanguinetti L, 2020a. Holographic MIMO communications under spatially-stationary scattering. Proc 54th Asilomar Conf on Signals, Systems, and Computers, p.702-706. https://doi.org/10.1109/IEEECONF51394.2020.9443506

Pizzo A, Marzetta TL, Sanguinetti L, 2020b. Spatially-stationary model for holographic MIMO small-scale fading. *IEEE J Sel Areas Commun*, 38(9):1964-1979. https://doi.org/10.1109/JSAC.2020.3000877

Pizzo A, Sanguinetti L, Marzetta TL, 2022a. Fourier plane-wave series expansion for holographic MIMO communications. *IEEE Trans Wirel Commun*, 21(9):6890-6905. https://doi.org/10.1109/TWC.2022.3152965

Pizzo A, Torres ADJ, Sanguinetti L, et al., 2022b. Nyquist sampling and degrees of freedom of electromagnetic fields. *IEEE Trans Signal Process*, 70:3935-3947. https://doi.org/10.1109/TSP.2022.3183445

Pizzo A, Sanguinetti L, Marzetta TL, 2022c. Spatial characterization of electromagnetic random channels. *IEEE Open J Commun Soc*, 3:847-866. https://doi.org/10.1109/OJCOMS.2022.3171409

Ramezani P, Kosasih A, Irshad A, et al., 2023. Exploiting the depth and angular domains for massive near-field spatial multiplexing. *IEEE BITS Inform Theory Mag*, 3(1):14-26. https://doi.org/10.1109/MBITS.2023.3322670

Raschkowski L, Kyösti P, Kusume K, et al., 2015. METIS Channel Models. Technical Report No. ICT-317669-METIS/D1.4 Ver3, ICT. https://www.researchgate.net/publication/282807948_METIS_Channel_Models_D14

Rogalin R, Bursalioglu OY, Papadopoulos H, et al., 2014. Scalable synchronization and reciprocity calibration for distributed multiuser MIMO. *IEEE Trans Wirel Commun*, 13(4):1815-1831. https://doi.org/10.1109/twc.2014.030314.130474

Sasaki H, Lee D, Fukumoto H, et al., 2018. Experiment on over-100-Gbps wireless transmission with OAM-MIMO multiplexing system in 28-GHZ band. Proc IEEE Global Communications Conf, p.1-6. https://doi.org/10.1109/GLOCOM.2018.8647361

Selvan KT, Janaswamy R, 2017. Fraunhofer and Fresnel distances: unified derivation for aperture antennas. *IEEE Antenn Propag Mag*, 59(4):12-15. https://doi.org/10.1109/MAP.2017.2706648

Sherman J, 1962. Properties of focused apertures in the Fresnel region. *IRE Trans Antenn Propag*, 10(4):399-408. https://doi.org/10.1109/TAP.1962.1137900

Shtaiwi E, Zhang HL, Vishwanath S, et al., 2021. Channel estimation approach for RIS assisted MIMO systems. *IEEE Trans Cogn Commun Netw*, 7(2):452-465. https://doi.org/10.1109/TCCN.2021.3075413

Shuang Y, Zhao HT, Ji W, et al., 2020. Programmable high-order OAM-carrying beams for direct-modulation wireless communications. *IEEE J Emerg Sel Top Circ Syst*, 10(1):29-37. https://doi.org/10.1109/JETCAS.2020.2973391

Sun S, Li RW, Han C, et al., 2023. How to differentiate between near field and far field: revisiting the Rayleigh distance. https://arxiv.org/abs/2309.13238

Tan JD, Su Z, Long YL, 2015. A full 3-D GPU-based beam-tracing method for complex indoor environments propagation modeling. *IEEE Trans Antenn Propag*, 63(6):2705-2718. https://doi.org/10.1109/TAP.2015.2415036

Tarboush S, Ali A, Al-Naffouri TY, 2024. Cross-field channel estimation for ultra massive-MIMO THz systems. *IEEE Trans Wirel Commun*, 23(8):8619-8635. https://doi.org/10.1109/TWC.2024.3352894

Thidé B, Then H, Sjöholm J, et al., 2007. Utilization of photon orbital angular momentum in the low-frequency radio domain. *Phys Rev Lett*, 99(8):087701. https://doi.org/10.1103/PhysRevLett.99.087701

Verdu S, 2002. Spectral efficiency in the wideband regime. *IEEE Trans Inform Theory*, 48(6):1319-1343. https://doi.org/10.1109/TIT.2002.1003824

Wang C, Zhang JH, Tian L, et al., 2017. The spatial evolution of clusters in massive MIMO mobile measurement at 3.5 GHz. Proc IEEE 85th Vehicular Technology Conf, p.1-6. https://doi.org/10.1109/VTCSpring.2017.8108242

Wang H, Wang WM, Zhang FC, et al., 2024. On efficient echo suppression with phaseless data in the joint frequency and spatial domain for antenna pattern measurement in a non-anechoic chamber. *IEEE Trans Antenn Propag*, 72(3):2968-2973. https://doi.org/10.1109/TAP.2024.3352274

Wang HZ, Zeng Y, 2022. SNR scaling laws for radio sensing with extremely large-scale MIMO. IEEE Int Conf on Communications Workshops, p.121-126. https://doi.org/10.1109/ICCWorkshops53468.2022.9814501

Wang HZ, Zeng Y, 2023. Can sparse arrays outperform collocated arrays for future wireless communications? IEEE Globecom Workshops, p.667-672. https://doi.org/10.1109/GCWkshps58843.2023.10465094

Wang HZ, Xiao ZQ, Zeng Y, 2024a. Cramér-Rao bounds for near-field sensing with extremely large-scale MIMO. *IEEE Trans Signal Process*, 72:701-717. https://doi.org/10.1109/TSP.2024.3350329

Wang HZ, Feng C, Zeng Y, et al., 2024b. Enhancing spatial multiplexing and interference suppression for near- and far-field communications with sparse MIMO. https://arxiv.org/abs/2408.01956

Wang JF, Ma Y, Yi N, et al., 2022. Network-ELAA beamforming and coverage analysis for eMBB/URLLC in spatially non-stationary Rician channels. IEEE Int Conf on Communications, p.3508-3513. https://doi.org/10.1109/ICC45855.2022.9839081

Wang P, Li YH, Yuan XJ, et al., 2014. Tens of gigabits wireless communications over E-band LoS MIMO channels with uniform linear antenna arrays. *IEEE Trans Wirel Commun*, 13(7):3791-3805.

https://doi.org/10.1109/TWC.2014.2318053

Wang Q, Ai B, Matolak DW, et al., 2017. Spatial variation analysis for measured indoor massive MIMO channels. *IEEE Access*, 5:20828-20840. https://doi.org/10.1109/ACCESS.2017.2736522

Wei L, Huang CW, Alexandropoulos GC, et al., 2023. Tri-polarized holographic MIMO surfaces for near-field communications: channel modeling and precoding design. *IEEE Trans Wirel Commun*, 22(12):8828-8842. https://doi.org/10.1109/TWC.2023.3266298

Wu CY, You CS, Liu YW, et al., 2024. Two-stage hierarchical beam training for near-field communications. *IEEE Trans Veh Technol*, 73(2):2032-2044. https://doi.org/10.1109/TVT.2023.3311868

Wu QQ, Zhang R, 2019. Intelligent reflecting surface enhanced wireless network via joint active and passive beamforming. *IEEE Trans Wirel Commun*, 18(11):5394-5409. https://doi.org/10.1109/TWC.2019.2936025

Wu ZD, Dai LL, 2023. Multiple access for near-field communications: SDMA or LDMA? *IEEE J Sel Areas Commun*, 41(6):1918-1935. https://doi.org/10.1109/JSAC.2023.3275616

Wu ZD, Cui MY, Dai LL, 2023. Enabling more users to benefit from near-field communications: from linear to circular array. *IEEE Trans Wirel Commun*, 23(4):3735-3748. https://doi.org/10.1109/TWC.2023.3310912

Xiao J, Wang J, Chen Z, et al., 2023. U-MLP-based hybrid-field channel estimation for XL-RIS assisted millimeter-wave MIMO systems. *IEEE Wirel Commun Lett*, 12(6): 1042-1046. https://doi.org/10.1109/10.1109/LWC.2023.3259465

Xie ZY, Liu YW, Xu JQ, et al., 2023. Performance analysis for near-field MIMO: discrete and continuous aperture antennas. *IEEE Wirel Commun Lett*, 12(12):2258-2262. https://doi.org/10.1109/LWC.2023.3317492

Xu HQ, Zhao YJ, Mo LM, et al., 2012. Inter-cell antenna calibration for coherent joint transmission in TDD system. IEEE Globecom Workshops, p.297-301. https://doi.org/10.1109/GLOCOMW.2012.6477586

Xu HX, Tang P, Zhang JH, et al., 2024. An empirical study on near-field, spatial non-stationarity, and beam misalignment characteristics of THz XL-MIMO channels at 132 GHz. IEEE Int Conf on Communications Workshops, p.744-749. https://doi.org/10.1109/ICCWorkshops59551.2024.10615710

Xu P, Zhang KY, Liu HX, et al., 2023. Dual-band metasurface generating multiple OAM beams independently in full polarizations. *Opt Expr*, 31(20):32637-32651. https://doi.org/10.1364/OE.497975

Xue H, Zhang S, Zhao SH, et al., 2022a. Generation of the Airy beam based on the truncated asymptotic expression of the Airy function using a transmissive metasurface. *Opt Expr*, 30(24):43842-43851. https://doi.org/10.1364/OE.472207

Xue H, Li RJ, Xu P, et al., 2022b. Model construction, theoretical analysis, and miniaturized implementation of high-order deflected multivortex beams with uniform elliptical array. *IEEE Trans Antenn Propag*, 70(8):7234-7239. https://doi.org/10.1109/TAP.2022.3164238

Xue H, Han JQ, Zhang S, et al., 2023. Co-modulation of spin angular momentum and high-order orbital angular momentum based on anisotropic holographic metasurfaces. *IEEE Trans Antenn Propag*, 71(5):4594-4599. https://doi.org/10.1109/TAP.2023.3243795

Yaghjian A, 1986. An overview of near-field antenna measurements. *IEEE Trans Antenn Propag*, 34(1):30-45. https://doi.org/10.1109/TAP.1986.1143727

Yamada W, Kita N, Sugiyama T, et al., 2009. Plane-wave and vector-rotation approximation technique for reducing computational complexity to simulate MIMO propagation channel using ray-tracing. *IEICE Trans Commun*, E92-B(12): 3850-3860. https://doi.org/10.1587/transcom.E92.B.3850

Yang LJ, Sun S, Sha WEI, et al., 2023. Multi-feed multi-mode metasurface for independent orbital angular momentum communication in dual polarization. *Front Inform Technol Electron Eng*, 24(12):1776-1790. https://doi.org/10.1631/FITEE.2200471

Ye M, Liang X, Pan CH, et al., 2024. GAN based near-field channel estimation for extremely large-scale MIMO systems. https://arxiv.org/abs/2402.17281

Yu SX, Li L, Shi GM, et al., 2016. Design, fabrication, and measurement of reflective metasurface for orbital angular momentum vortex wave in radio frequency domain. *Appl Phys Lett*, 108(12):1211903. https://doi.org/10.1063/1.4944789

Yu SX, Li L, Kou N, 2017. Generation, reception and separation of mixed-state orbital angular momentum vortex beams using metasurfaces. *Opt Mater Expr*, 7(9):3312-3321. https://doi.org/10.1364/OME.7.003312

Yu WT, Shen YF, He HT, et al., 2023. An adaptive and robust deep learning framework for THz ultra-massive MIMO channel estimation. *IEEE J Sel Top Signal Process*, 17(4): 761-776. https://doi.org/10.1109/JSTSP.2023.3282832

Yuan YF, Zhao YJ, Zong BQ, et al., 2020. Potential key technologies for 6G mobile communications. *Sci China Inform Sci*, 63(8):183301. https://doi.org/10.1007/s11432-019-2789-y

Yuan ZQ, Zhang JH, Ji YL, et al., 2023a. Spatial non-stationary near-field channel modeling and validation for massive MIMO systems. *IEEE Trans Antenn Propag*, 71(1):921-933. https://doi.org/10.1109/TAP.2022.3218759

Yuan ZQ, Zhang FC, Zhang YX, et al., 2023b. On phase mode selection in the frequency-invariant beamformer for near-field mmWave channel characterization. *IEEE Trans Antenn Propag*, 71(11):8975-8986. https://doi.org/10.1109/TAP.2023.3316791

Yuan ZQ, Lyu YJ, Zhang JH, et al., 2023c. Sub-THz ray tracing simulation and experimental validation for indoor scenarios. IEEE Int Mediterranean Conf on Communications and Networking, p.7-11. https://doi.org/10.1109/10.1109/MeditCom58224.2023.10266598

Yuan ZQ, Zhang JH, Degli-Esposti V, et al., 2024. Efficient ray-tracing simulation for near-field spatial non-stationary mmWave massive MIMO channel and its experimental validation. *IEEE Trans Wirel Commun*, 23(8):8910-8923. https://doi.org/10.1109/TWC.2024.3357071

Yue SH, Zeng SH, Liu L, et al., 2023. Channel estimation for holographic communications in hybrid near-far field. Proc IEEE Global Communications Conf, p.6133-6138. https://doi.org/10.1109/GLOBECOM54140.2023.10436807

Zhang FC, Fan W, 2019. Near-field ultra-wideband mmWave channel characterization using successive cancellation beamspace UCA algorithm. *IEEE Trans Veh Technol*, 68(8): 7248-7259. https://doi.org/10.1109/TVT.2019.2926783

Zhang HY, Shlezinger N, Guidi F, et al., 2022. Beam focusing for near-field multiuser MIMO communications. *IEEE Trans Wirel Commun*, 21(9):7476-7490. https://doi.org/10.1109/TWC.2022.3158894

Zhang J, Yang G, Ye QB, et al., 2024. Low-complexity joint azimuth-range-velocity estimation for integrated sensing and communication with OFDM waveform. https://arxiv.org/abs/2405.09443

Zhang JH, Zhang YX, Yu YW, et al., 2017. 3-D MIMO: how much does it meet our expectations observed from channel measurements? *IEEE J Sel Areas Commun*, 35(8): 1887-1903. https://doi.org/10.1109/JSAC.2017.2710758

Zhang JH, Zheng Z, Zhang YX, et al., 2018. 3D MIMO for 5G NR: several observations from 32 to massive 256 antennas based on channel measurement. *IEEE Commun Mag*, 56(3): 62-70. https://doi.org/10.1109/MCOM.2018.1700846

Zhang JH, Lin JX, Tang P, et al., 2024a. Deterministic ray tracing: a promising approach to THZ channel modeling in 6G deployment scenarios. *IEEE Commun Mag*, 62(2):48-54. https://doi.org/10.1109/MCOM.001.2200486

Zhang JH, Miao HY, Tang P, et al., 2024b. New mid-band for 6G: several considerations from the channel propagation characteristics perspective. *IEEE Commun Mag*, 63(1): 175-180. https://doi.org/10.1109/MCOM.001.2300708

Zhang P, Chen JQ, Yang XL, et al., 2018. Recent research on massive MIMO propagation channels: a survey. *IEEE Commun Mag*, 56(12):22-29. https://doi.org/10.1109/MCOM.2018.1800196

Zhang S, Di B, Zhang H, et al., 2024. Hierarchical codebook design using scale-changeable reconfigurable holographic surfaces in near-far field communications. Proc IEEE Global Commun Conf.

Zhang SP, Zhang YT, Di BY, 2023. Near-far field codebook design for IOS-aided multi-user communications. IEEE Global Communications Conf, p.2888-2893. https://doi.org/10.1109/GLOBECOM54140.2023.10436845

Zhang X, Zhang HY, Eldar YC, 2024. Near-field sparse channel representation and estimation in 6G wireless communications. *IEEE Trans Commun*, 72(1):450-464. https://doi.org/10.1109/TCOMM.2023.3322449

Zhang XY, Wang ZN, Zhang HY, et al., 2023. Near-field channel estimation for extremely large-scale array communications: a model-based deep learning approach. *IEEE Commun Lett*, 27(4):1155-1159. https://doi.org/10.1109/LCOMM.2023.3245084

Zhang Y, Alkhateeb A, 2023. Deep learning of near field beam focusing in terahertz wideband massive MIMO systems. *IEEE Wirel Commun Lett*, 12(3):535-539. https://doi.org/10.1109/LWC.2022.3233566

Zhang YC, Zhang HY, Xiao S, et al., 2024. Near-field wideband secure communications: an analog beamfocusing approach. *IEEE Trans Signal Process*, 72:2173-2187. https://doi.org/10.1109/TSP.2024.3390177

Zhang YT, Di BY, Zhang HL, et al., 2022. Codebook design for large reconfigurable refractive surface enabled holographic MIMO systems. Proc IEEE Global Communications Conf, p.639-644. https://doi.org/10.1109/GLOBECOM48099.2022.10001733

Zhang YT, Di BY, Zhang HL, et al., 2023. Near-far field beamforming for holographic multiple-input multiple-output. *J Commun Inform Netw*, 8(2):99-110. https://doi.org/10.23919/JCIN.2023.10173734

Zhang Z, Zhang JH, Zhang YX, et al., 2023. Deep reinforcement learning based dynamic beam selection in dual-band communication systems. *IEEE Trans Wirel Commun*, 23(4):2591-2606. https://doi.org/10.1109/TWC.2023.3300830

Zhang Z, Liu YW, Wang ZL, et al., 2024. Physical layer security in near-field communications. *IEEE Trans Veh Technol*, 73(7):10761-10766. https://doi.org/10.1109/TVT.2024.3366115

Zhao YJ, 2023. Reconfigurable intelligent surfaces for 6G: applications, challenges, and solutions. *Front Inform Technol Electron Eng*, 24(12):1669-1688. https://doi.org/10.1631/FITEE.2200666

Zhao YJ, 2024a. Cascaded channel decoupling based solution for RIS regulation matrix. *Intell Converg Netw*, 5(1):19-27. https://doi.org/10.23919/ICN.2024.0002

Zhao YJ, 2024b. Reconfigurable intelligent surface constructing 6G near-field networks. *Mob Commun*, 48(4):1-11 (in Chinese). https://doi.org/10.3969/j.issn.1006-1010.20240327-0003

Zhao YJ, 2024c. RIS constructing 6G near-field networks: opportunities and challenges. https://arxiv.org/abs/2403.15390

Zhao YJ, 2024d. RIS assisted wireless networks: collaborative regulation, deployment mode and field testing. *IET Commun*, 18:1665-1682. https://doi.org/10.1049/cmu2.12808

Zhao YJ, Jian MN, 2021. Applications and challenges of reconfigurable intelligent surface for 6G networks. https://arxiv.org/abs/2108.13164

Zhao YJ, Lv X, 2022. Network coexistence analysis of RIS-assisted wireless communications. *IEEE Access*, 10: 63442-63454. https://doi.org/10.1109/ACCESS.2022.3183139

Zhao YJ, Yu GH, Xu HQ, 2019. 6G mobile communication networks: vision, challenges, and key technologies. *Sci Sin*

Inform, 49(8):963-987. https://doi.org/10.1360/N112019-00033

Zhao YJ, Dai LL, Zhang JH, et al., 2024. 6G Near-Field Technologies White Paper. FuTURE Forum, Nanjing, China. https://doi.org/10.12142/FuTURE.202404002

Zheng BX, Zhang R, 2022. Simultaneous transmit diversity and passive beamforming with large-scale intelligent reflecting surface. *IEEE Trans Wirel Commun*, 22(2):920-933. https://doi.org/10.1109/TWC.2022.3199426

Zheng BX, Ma TT, Yi X, et al., 2023. Intelligent reflecting surface-aided transmit diversity and performance analysis. IEEE Int Conf on Communications, p.2822-2827. https://doi.org/10.1109/ICC45041.2023.10279543

Zheng S, 2024. RIS(24)012008r3 (NWI), Reconfigurable Intelligent Surfaces: Near-Field Channel Modeling and Mechanics. ETSI ISG RIS. https://portal.etsi.org/webapp/WorkProgram/Report_WorkItem.asp?WKI_ID=70055

Zheng Z, Fu MC, Wang WQ, et al., 2018. Mixed far-field and near-field source localization based on subarray cross-cumulant. *Signal Process*, 150:51-56. https://doi.org/10.1016/j.sigpro.2018.03.020

Zhi KD, Pan CH, Ren H, et al., 2024. Performance analysis and low-complexity design for XL-MIMO with near-field spatial non-stationarities. *IEEE J Sel Areas Commun*, 42(6):1656-1672. https://doi.org/10.1109/JSAC.2024.3389128

Zhou KZ, He SL, Hong SH, et al., 2020. Spontaneous-focusing and self-healing of Airy-like beams. *Results Phys*, 19: 103526. https://doi.org/10.1016/j.rinp.2020.103526

Zhou Z, Gao X, Fang J, et al., 2015. Spherical wave channel and analysis for large linear array in LoS conditions. Proc IEEE Globecom Workshops, p.1-6. https://doi.org/10.1109/GLOCOMW.2015.7414041

Zhu LP, Ma WY, Zhang R, 2023. Movable antennas for wireless communication: opportunities and challenges. *IEEE Commun Mag*, 62(6):114-120. https://doi.org/10.1109/MCOM.001.2300212

Zhuo BT, Gu JP, Duan W, et al., 2024. Extremely large-scale array system: cooperative NFC or FFC? *IEEE Wirel Commun Lett*, 13(5):1250-1254. https://doi.org/10.1109/LWC.2024.3367132

ZTE, 2011. R1-112261 Evaluation on the Impact of Timing Error between CoMP Transmission Points. https://www.3gpp.org/ftp/tsg_ran/WG1_RL1/TSGR1_66/Docs/R1-112261.zip